

# Lanthanum Gallate as a New SOFC Electrolyte

John B. Goodenough (jgoodenough@mail.utexas.edu, (512) 471-1646))

Kequin Huang (khuang@mail.utexas.edu, (512) 471-3588))

Center for Materials Science & Engineering

University of Texas at Austin

Bldg. ETC 9.102

Austin, TX 78712-1063

## Abstract

The single-phase, cubic-perovskite region of the  $\text{LaO}_{1.5}\text{-SrO-GaO}_{1.5}\text{-MgO}$  phase diagram has been determined from room-temperature and high-temperature x-ray diffraction. Two impurity phases were identified,  $\text{LaSrGaO}_4$  and  $\text{LaSrGa}_3\text{O}_7$ . An essentially pure oxide-ion conductivity of the oxygen-deficient perovskite phase was formed over the wide range  $10^{-22} \leq \text{Po}_2 \leq 1$  atm of oxygen partial pressures. The highest values of  $\sigma_o$  were found for  $\text{La}_{0.8}\text{Sr}_{0.2}\text{Ga}_{0.83}\text{Mg}_{0.17}\text{O}_{2.815}$  with  $\sigma_o = 0.17$  S/cm and 0.08 S/cm at 800°C and 700°C, respectively. The oxide-ion conductivities remained stable over a week-long test. The Arrhenius plot of  $\sigma_o$  is curved, dividing into two straight-line regions with different activation energies above and below a critical temperature  $T^* = 600^\circ\text{C}$ . This behavior is well-described by a model in which all the oxygen vacancies are mobile at temperature  $T > T^*$ , but they progressively condense into clusters of ordered vacancies with decreasing temperature  $T < T^*$ .

SEM microstructures of samples  $\text{La}_{1.8}\text{Sr}_{0.2}\text{Ga}_{1-y}\text{Mg}_y\text{O}_{2.9-0.5y}$ ,  $0.05 \leq y \leq 0.30$ , were obtained after thermal etching at 1350°C for 2 h. Smaller grain sizes were found in the two-phase regions. The impurity  $\text{LaSrGa}_3\text{O}_7$  appearing for  $0.05 \leq y \leq 0.10$  is seen distributed over the grain boundaries. The impurity  $\text{LaSrGaO}_4$ , existing in samples with  $0.25 \leq y \leq 0.30$ , melts at 1400°C and is in a molten state at the sintering temperature 1470°C; it therefore acts as a flux and appears to drain away from the grain boundaries to form globular second-phase regions at grain-boundary intersections. TEM micrographs show well-bonded grain-boundary interfaces where x-ray diffraction shows a  $\text{LaSrGaO}_4$  second phase.

AC-impedance spectroscopy was used to investigate the grain-boundary contribution to the DC resistance and the influence of impurities on this contribution. The impurity  $\text{LaSrGa}_3\text{O}_7$  in samples  $0.05 \leq y \leq 0.10$  contributed to a perfect or a depressed grain-boundary semicircle in the complex-impedance plane. The depressed semicircle represents a constant-phase element (CPE) indicative of an oxide-ion insulator, *viz.*, the  $\text{LaSrGa}_3\text{O}_7$  impurity, at the grain boundary. This grain-boundary semicircle vanishes if a hydrogen-containing atmosphere is applied, which indicates good proton conduction across the impurity phase at the grain boundaries. In contrast, the impurity  $\text{LaSrGaO}_4$  seen in samples with  $0.25 \leq y \leq 0.30$  gives no grain-boundary contribution to the impedance; in fact, the grain-boundary semicircle vanishes in these samples.

The performance of the optimized electrolyte  $\text{La}_{0.8}\text{Sr}_{0.2}\text{Ga}_{0.83}\text{Mg}_{0.17}\text{O}_{2.815}$  (LSGM) in a SOFC was tested on single cells having a 500- $\mu\text{m}$ -thick electrolyte membrane and a

$\text{La}_{1-x}\text{Sr}_x\text{CoO}_{3.0}$  cathode. It was found that poor anode performance was due to a reactivity of the NiO in the composite NiO·CeO<sub>2</sub> or NiO·LSGM anodes with LSGM to form LaNiO<sub>3</sub> at the anode-electrolyte interface. To prevent this reaction, a thin Sm-doped CeO<sub>2</sub> layer was introduced between the electrolyte and the anode. Comparison of Sm:CeO<sub>2</sub>/Sm:CeO<sub>2</sub> + Ni and Sm:CeO<sub>2</sub> + Ni anodes showed that introduction of the Sm:CeO<sub>2</sub> interlayer gave an exchange-current density four times larger. The peak power density of the interlayered thick-electrolyte cell was 100 mW higher than a cell without the interlayer. The improvement was shown to be due to a reduction of the anode overpotential. Comparison of the peak power density in this study with that of a previous study, also with a 500- $\mu\text{m}$ -thick electrolyte, shows a factor of two improvements, *i.e.*, from 270 mW/cm<sup>2</sup> to 550 mW/cm<sup>2</sup> at 800°C. This excellent cell performance indicates that an LSGM-based SOFC operating in the temperature range 600°C < T<sub>op</sub> < 800°C is a realistic goal.

Electric Power Research Institute (EPRI)

Contract Number: W08062-08

Wate Bakker, COR

Two year total contract

# Lanthanum Gallate as a New SOFC Electrolyte

John B. Goodenough (jgoodenough@mail.utexas.edu, (512) 471-1646)  
Keqin Huang (kqhuang@mail.utexas.edu, (512) 471-3588)  
Center for Materials Science & Engineering  
The University of Texas at Austin  
Bldg ETC 9.102  
Austin, TX 78712-1063

## Executive Summary

With the identification of Sr- and Mg- doped  $\text{LaGaO}_3$  as a superior oxide-ion electrolyte, the task of this grant was to optimize the composition and to evaluate its suitability for use in a solid oxide fuel cell (SOFC).

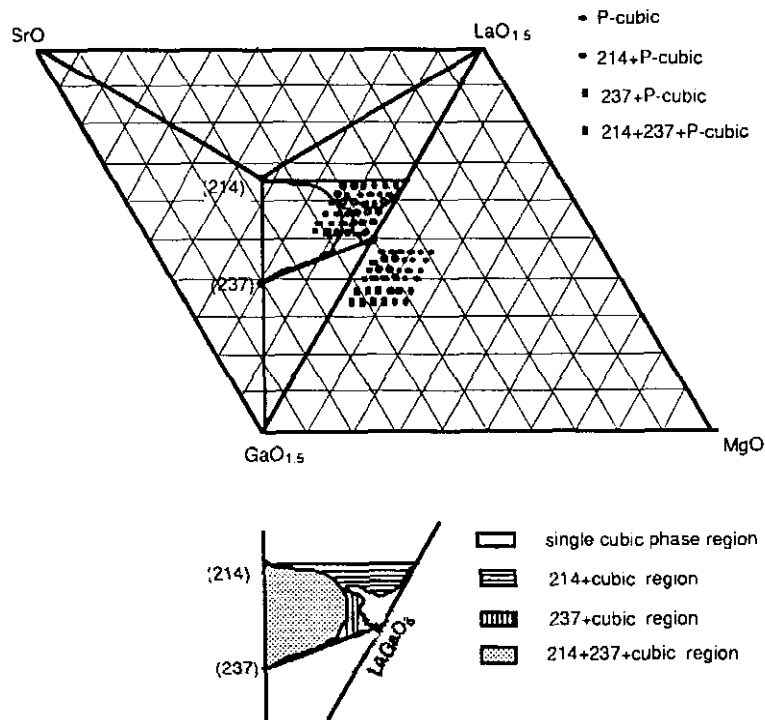


Fig. 1 Phase diagram of  $\text{LaO}_{1.5}$ -SrO- $\text{GaO}_{1.5}$ -MgO system

A quaternary phase diagram for  $\text{LaO}_{1.5}\text{-SrO-GaO}_{1.5}\text{-MgO}$  was determined, Fig. 1; a single perovskite phase was found to be restricted to a narrow range of compositions  $\text{La}_{1-x}\text{Sr}_x\text{Ga}_{1-y}\text{Mg}_y\text{O}_{3-0.5(x+y)}$ .  $\text{LaSrGa}_3\text{O}_7$  and  $\text{LaSrGaO}_4$  were identified as impurity phases condensing out at the grain boundaries or the pores; excess MgO precipitated in the grains. The system was also found to tolerate vacancies in the  $\text{La}_{1-x}\text{Sr}_x$ -cation subarray, thereby allowing a greater Mg substitution. Calcining of commercial "Mg carbonate" at 1000 °C for more than 3 hours was needed to obtain a reliable MgO starting material.

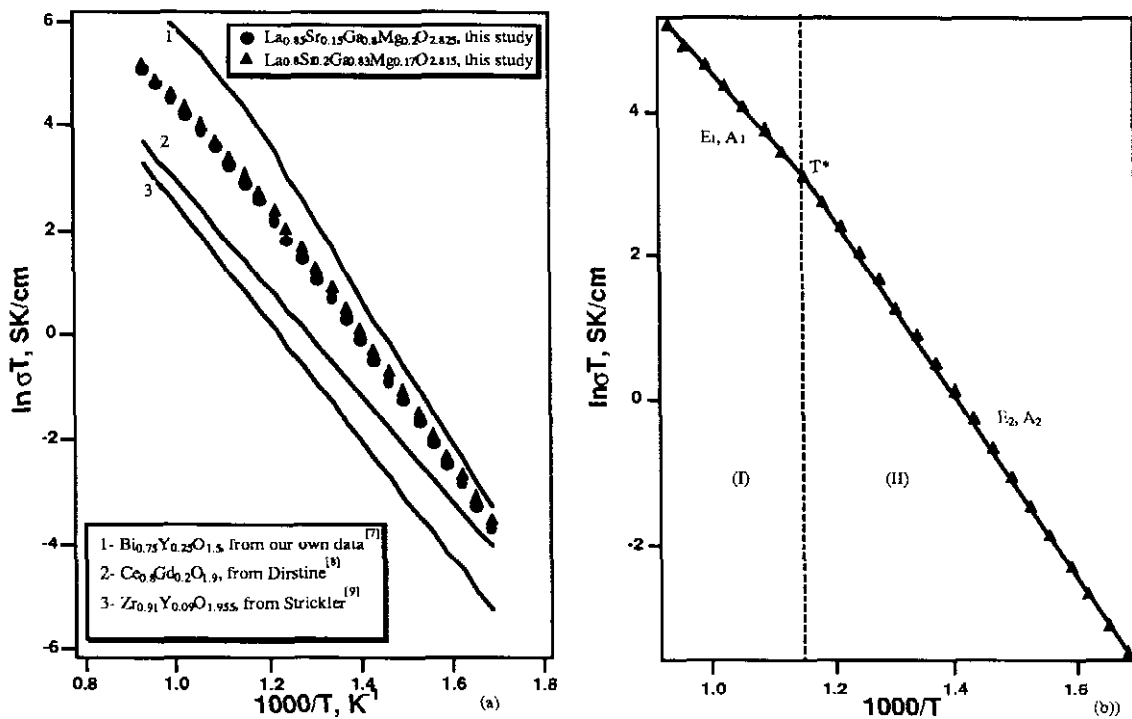


Fig. 2 (a) Arrhenius plots of conductivity for two typical compositions compared with other well-known oxide-ion conductor; (b) Separation into regions (I) and (II) at  $T^*$

Electrical measurements showed only oxide-ion conduction, without degradation in life tests, over the wide range of oxygen partial pressures existing in fuel cell operation ( $1 \leq P_{\text{O}_2} \leq 10^{-22}$  atm). Arrhenius plots, Fig. 2, of the oxide-ion conductivity  $\sigma_o$  versus reciprocal absolute temperature  $T$ ,  $\ln(\sigma_o T)$  vs  $1/T$ ,

distinguished two temperature regions: for  $T \geq T^* \approx 600$  °C,  $A=A_1$  and  $E_a = E_1$ ; for  $T < T^*$ ,  $A=A_2$  and  $E_a=E_2$  in the expression

$$\sigma_0 T = A \exp(-E_a/kT)$$

This behavior was interpreted with a model in which the oxygen vacancies are disordered above  $T^*$ , which makes  $E_1=\Delta H_m$ , the motional enthalpy, whereas below  $T^*$  the vacancies become progressively trapped out at a vacancy-ordered condensate by a trapping energy  $\Delta H_v$ , which makes  $E_2=\Delta H_m+\Delta H_v$  and  $A_2=A_1 \exp(\Delta H_v/kT^*)$ . At 800 °C, the region of highest oxide-ion conductivity,  $\sigma_0 > 0.14$  S/cm, falls in the compositional ranges  $0.125 \leq x \leq 0.25$  and  $0.125 \leq y \leq 0.25$ . The maximum oxide-ion conductivities found at 800 °C, Fig. 3, 700 °C, and 600 °C were, respectively, 0.17, 0.08 and 0.03 S/cm for  $\text{La}_{0.8}\text{Sr}_{0.2}\text{Ga}_{0.83}\text{Mg}_{0.17}\text{O}_{2.825}$ .

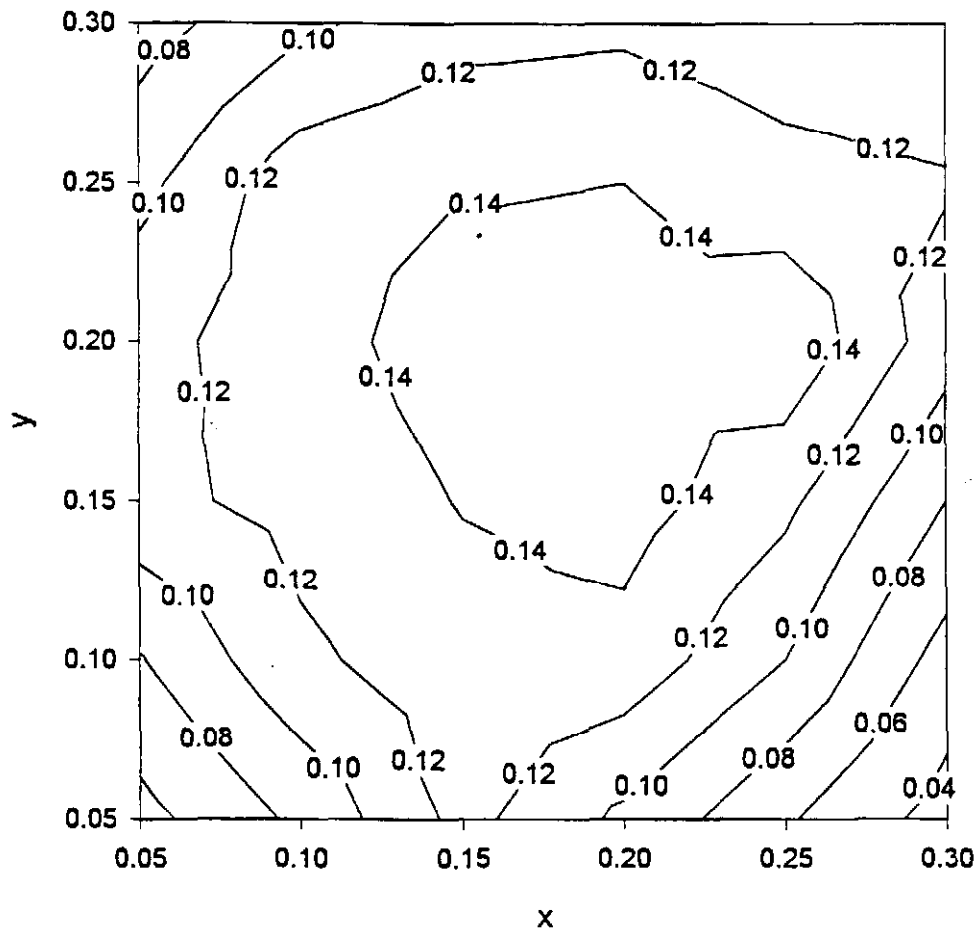


Fig. 3 Isoconductivity diagram of  $\text{La}_{1-x}\text{Sr}_x\text{Ga}_{1-y}\text{Mg}_y\text{O}_{3-0.5(x+y)}$  at 800 °C

SEM microstructures of samples with  $x = 0.20$  showed precipitation of  $\text{LaSrGa}_3\text{O}_7$  over the grain boundaries for  $y \leq 0.10$  and  $\text{LaSrGaO}_4$  particles pinning the grain boundary for  $y \geq 0.25$ ; in addition, intragranular  $\text{MgO}$  precipitates were found for  $y = 0.30$ . AC-impedance spectroscopy showed an important grain-boundary contribution to the oxide-ion impedance for  $y \leq 0.10$ , but no grain-boundary contribution for larger values of  $y$ . The  $\text{LaSrGaO}_4$  phase is liquid at the sintering temperature and promotes strong intergranular bonding.

Three soft-chemical routes for the synthesis of high-purity, ultra-homogeneous  $\text{La}_{1-x}\text{Sr}_x\text{Ga}_{1-y}\text{Mg}_y\text{O}_{3-0.5(x+y)}$  powders were compared; the sol-gel process, co-precipitation, and hydrothermal reaction. Powders produced by these routes reduce the sintering temperature required for materials processing. The powders obtained were characterized by x-ray diffraction, thermal analysis, transmission electron microscopy, and fourier-transformed infrared spectroscopy in order to elucidate the reaction mechanisms operating in each synthesis. The electrolyte could be prepared as a single phase by both the sol-gel and the Pechini co-precipitation methods, but not by hydrothermal treatment.

Chemical compatibility between the electrodes and the electrolyte were investigated by monitoring with EDS the diffusion of cations across the interface between them. Conventional cathodes were studied: porous  $\text{La}_{1-x}\text{Sr}_x\text{MnO}_3$  and films of  $\text{La}_{1-x}\text{Sr}_x\text{CoO}_{3-\delta}$ . The former did not react with the electrolyte; the latter interdiffused at higher temperature, but not appreciably at an operating temperature of  $800^\circ\text{C}$ . An electrode that conducts both oxide ions and electrons allows use of an electrode film; an electrode that conducts only electrons must be made as a thick, porous layer.  $\text{La}_{1-x}\text{Sr}_x\text{MnO}_3$  has a thermal expansion compatible with the electrolyte, but it only conducts electrons.  $\text{La}_{1-x}\text{Sr}_x\text{CoO}_{3-\delta}$  conducts both electrons and oxide ions, but it has an anomalously large thermal expansion. Nevertheless, we used  $\text{La}_{1-x}\text{Sr}_x\text{CoO}_{3-\delta}$  cathodes in our fuel-cell tests because of its excellent mixed electronic and oxide-ion conduction.

Conventional anodes are formed from composites of NiO with either the electrolyte or  $Ce_{1-x}Sm_xO_{2-0.5x}$ . The reducing atmosphere at an anode reduces the NiO to elemental Ni deposited on the walls of a porous structure. However, we found that interdiffusion of Ni and Ga across the electrode-electrolyte interface introduces at the interface metallic  $LaNiO_3$ , which blocks oxide-ion conduction. To circumvent this problem, we introduced  $Ce_{1-x}Sm_xO_{2-0.5x}$  which conducts both oxide ions and electrons in a reducing atmosphere, as a thin buffer layer between the electrolyte and a  $Ce_{1-x}Sm_xO_{2-0.5x} + NiO$  anode.

Single fuel cells were constructed for testing. Introduction of the buffer layer at the anode reduced significantly the anode overpotential and extended the life of the cell, Table 1. With a 500- $\mu$ m-thick electrolyte, maximum power densities of 550 mW/cm<sup>2</sup> at 1.1A/cm<sup>2</sup> were obtained, Fig. 4. A life test showed a stable power output for at least a period of 1500 hours under a loading current 250 mA/cm<sup>2</sup>. Reducing the thickness of the electrolyte would greatly improve performance.

**Table 1 Resistances ( $\Omega$ ) at a frequency of 5Hz at 800 °C in the atmosphere of wet hydrogen**

time (h)	anodes	LSGM+NiO	Sm-CeO <sub>2</sub> / LSGM+NiO	CeO <sub>2</sub> +NiO	Sm-CeO <sub>2</sub> / Ca- CeO <sub>2</sub> +NiO
0		648	146	354	78
5		691	124	273	74
10		622	124	284	74
15		611	124	295	74
20		625	126	306	75

In conclusion, we have demonstrated that the  $La_{1-x}Sr_xGa_{1-y}Mg_yO_{3-0.5(x+y)}$  electrolyte promises to provide a SOFC operating at 800 °C with a thick-film (*ca.* 100  $\mu$ m) electrolyte, at 600 °C with a thin-film (*ca.* 10  $\mu$ m) electrolyte.

The fuel-cell tests reported were done in collaboration with Dr. Chris Milliken, Dr. Ashok Khankar and Dr. S. Elangovan of Ceramatec, Inc.. We are grateful for their valuable cooperation.

Sponsor: Electric Power Research Institute (EPRI)

Contract Number: WO 8062-08

Dr. Wate Bakker, COR

Two year total contract

**Keywords:** Solid electrolyte, oxide-ion; perovskite, lanthanum gallate; solid oxide fuel cell; phase diagram,  $\text{LaO}_{1.5}\text{-SrO-GaO}_{1.5}\text{-MgO}$ ; ionic conduction; buffer layer.

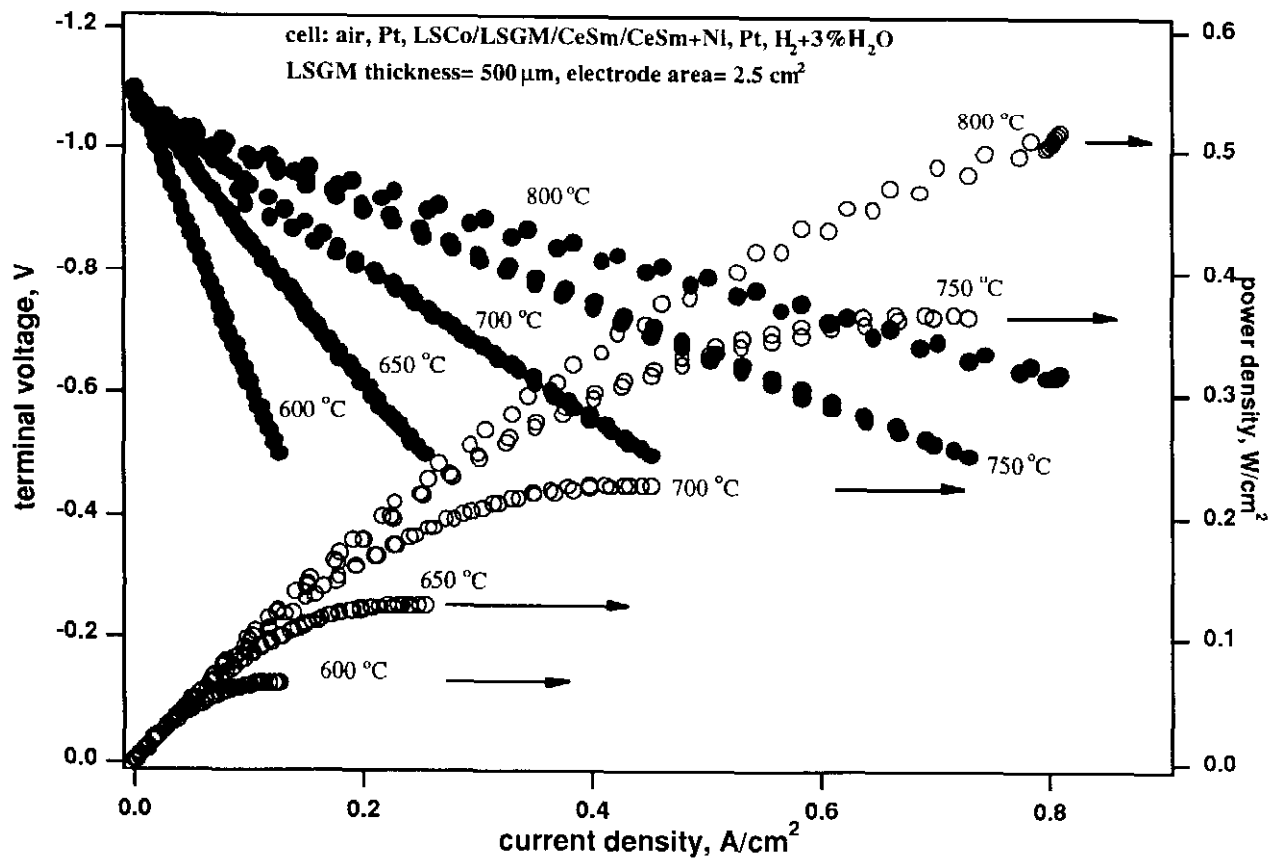


Fig. 4 Single fuel cell performance based on LSGM electrolyte with LSCo as cathode and  $\text{Sm-CeO}_2/\text{Sm-CeO}_2+\text{Ni}$  bilayer anode at different temperatures

---

# LANTHANUM GALLATE AS A NEW SOFC ELECTROLYTE

John B. Goodenough & Keqin Huang

EPRI Sponsor: Dr. Wate T. Bakker

# OUTLINE

---

- Optimal compositions in  $\text{La}_{1-x}\text{Sr}_x\text{Ga}_{1-y}\text{Mg}_y\text{O}_{3-0.5(x+y)}$  system
- Condensate of short-range order  $T < T^* \approx 600^\circ\text{C}$
- Microstructures and ac impedance spectroscopy
- Introduction of anode layer

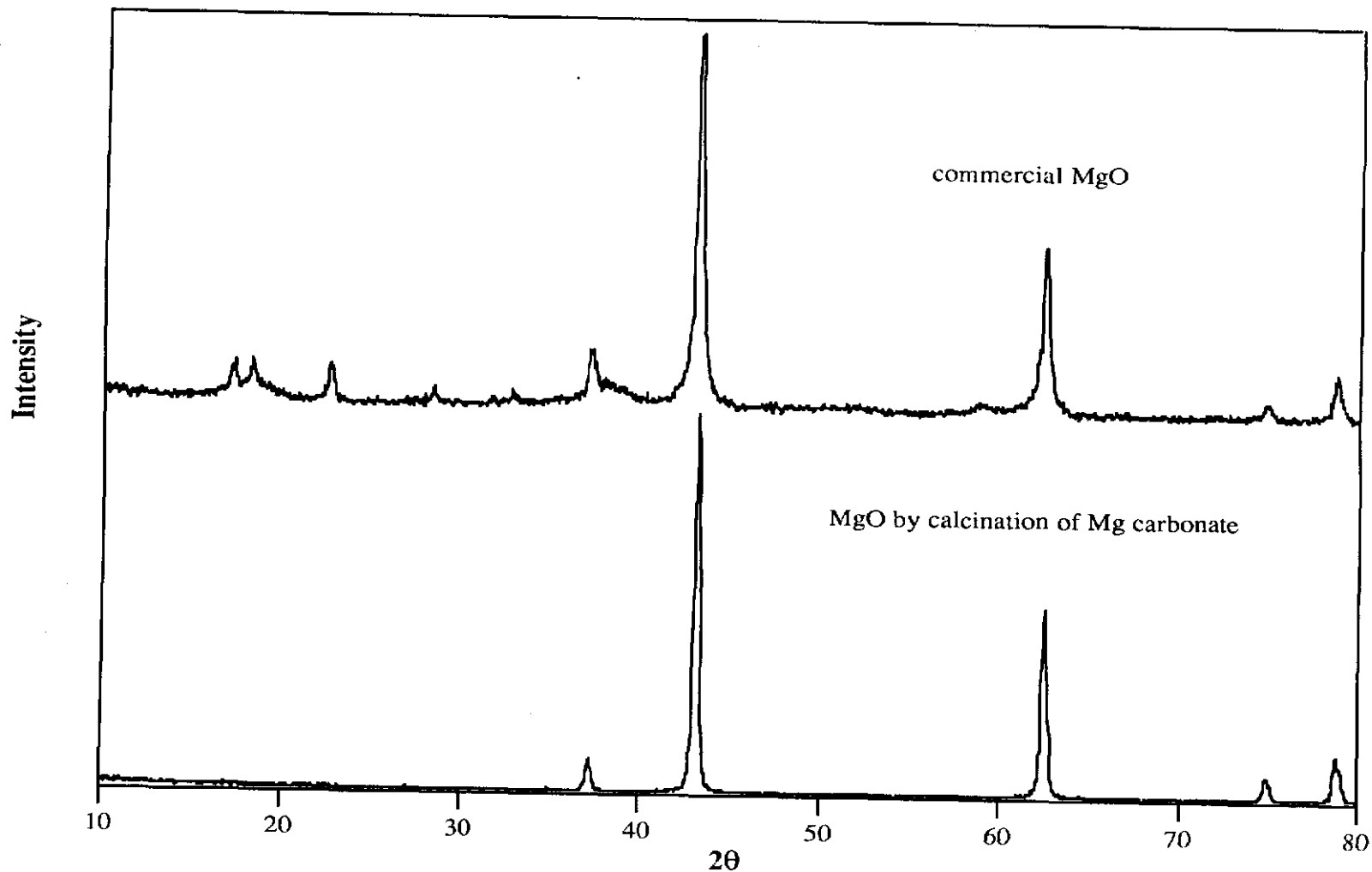
# SAMPLE PREPARATION

---

- Intimate mixing of  $\text{La}_2\text{O}_3$ ,  $\text{SrCO}_3$ ,  $\text{Ga}_2\text{O}_3$  and  $\text{MgO}^*$
- Pressed pellets fired overnight at 1250 °C
- Partially sintered pellets reground and ball-milled
- 6-mm-diameter x 5-7 mm pellets fired 24 h at 1470 °C

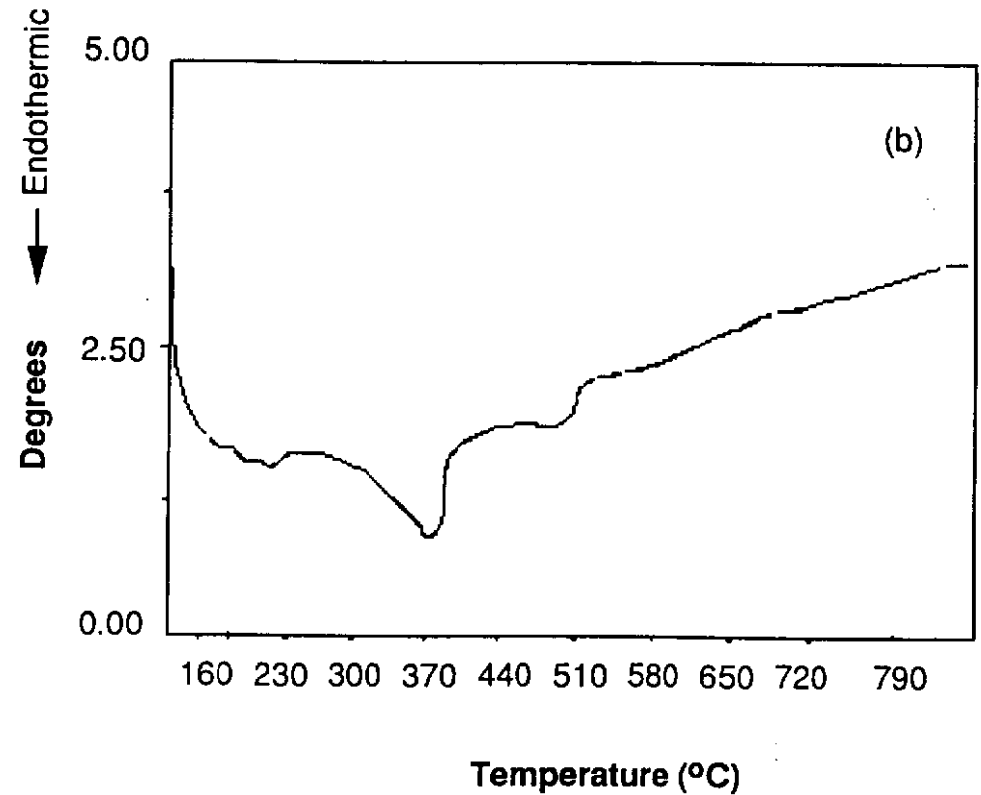
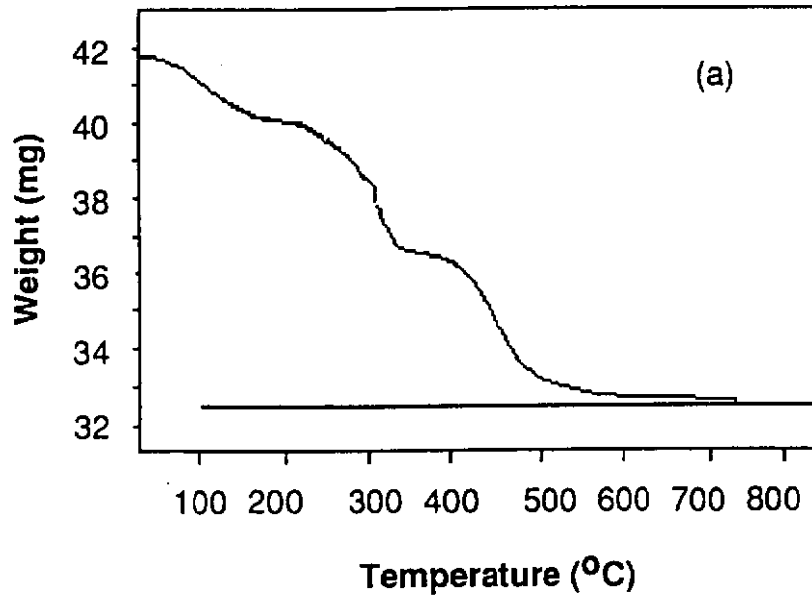
*\* after calcining Mg carbonate for 4 h at 1000 °C*

# XRD Patterns of Dried and Undried Commercial MgO



# TGA/DTA Curves of Commercial MgO

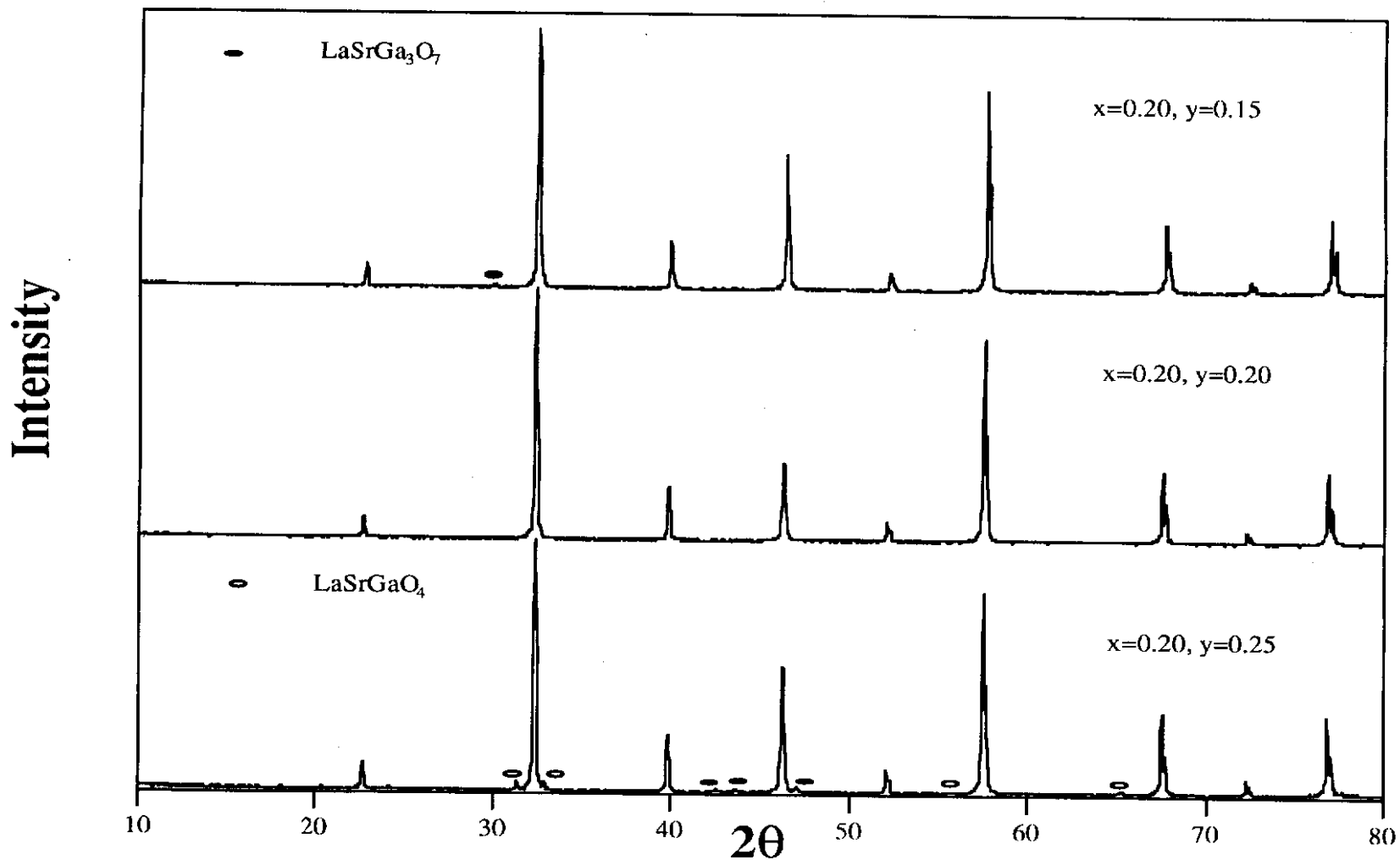
---



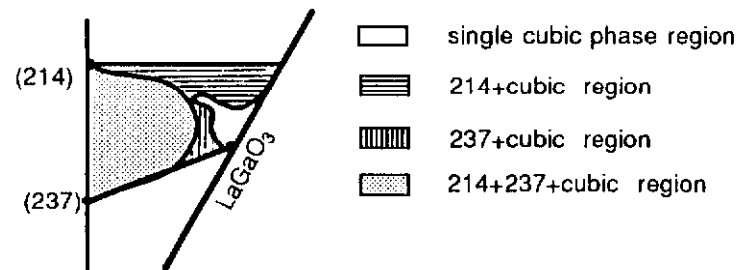
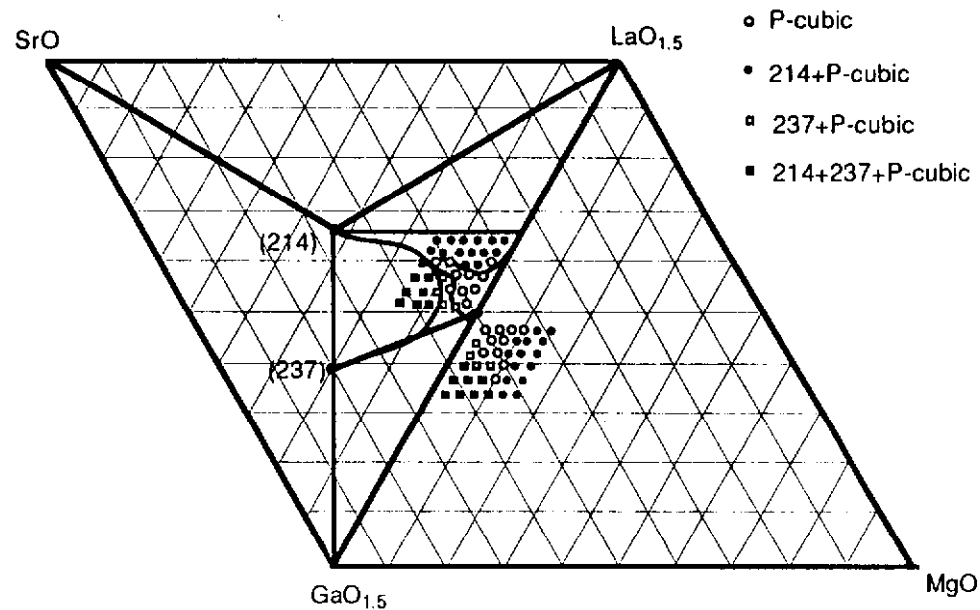
# XRD Patterns of

$$\text{La}_{0.8}\text{Sr}_{0.2}\text{Ga}_{1-y}\text{Mg}_y\text{O}_{3-0.5(0.2+y)}$$

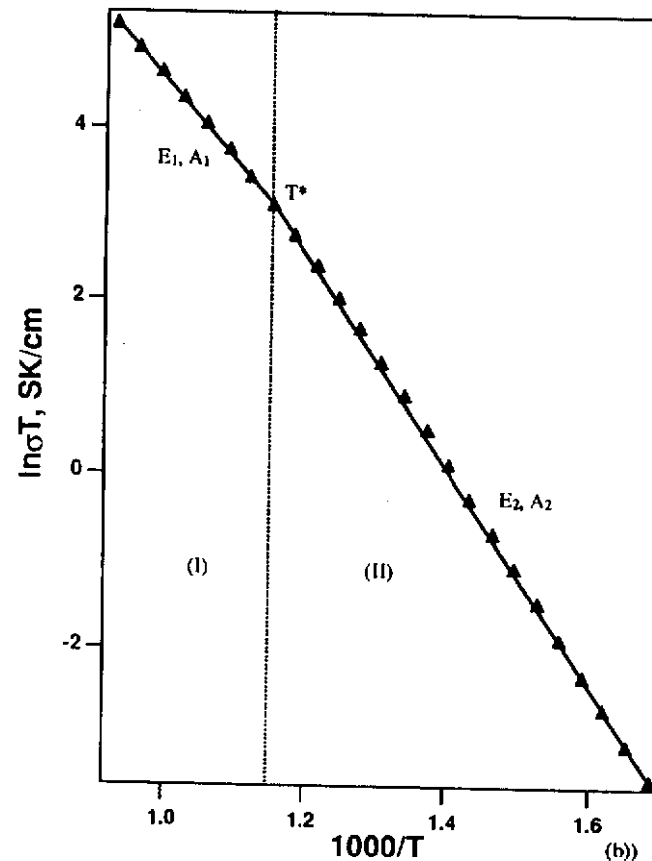
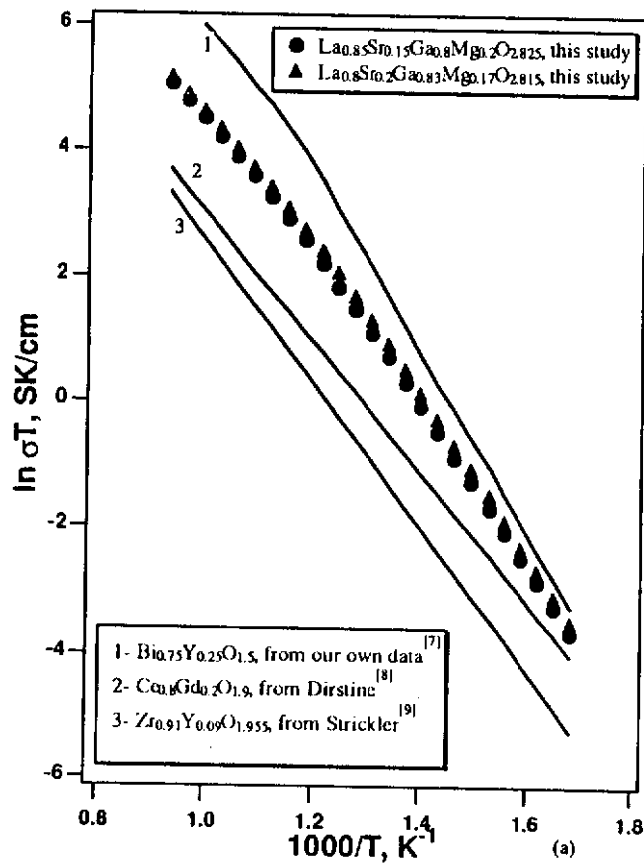
---



# Phase Diagram of LaO<sub>1.5</sub>-SrO-GaO<sub>1.5</sub>-MgO



# Conductivity vs Temperature



# IONIC CONDUCTIVITY

---

$$\mu_0 = qD/kT = (qD_0/kT)\exp(-\Delta G_m/kT)$$
$$\sigma_0 = cNq\mu_0 = (A/T)\exp(-E_a/kT)$$

Assume:

$T \geq T^*$ , vacancies disorder

$$\therefore E_a = E_1 = \Delta H_m, c=c^*, A=A_1$$

$T < T^*$ , vacancies progressively trapped  
in condensate

$$\ln(c/c^*) = -(\Delta H_t/kT)[1-(T/T^*)]$$

$$\therefore E_a = E_2 = \Delta H_m + \Delta H_t, A_2 = A_1 \exp(\Delta H_t/kT^*)$$

$$\ln(A_2/A_1) = \Delta H_t/kT^* = (E_2 - E_1)/kT^*$$

# PROOF

---

Let:

$\mu_V^*(\text{cond})$  = chemical potential of condensate

$\mu_V^0(\text{sol})$  = chemical potential of pure solid solution

$$\Delta G_t(T) = \mu_V^0(\text{sol}) - \mu_V^*(\text{cond})$$

At equilibrium:

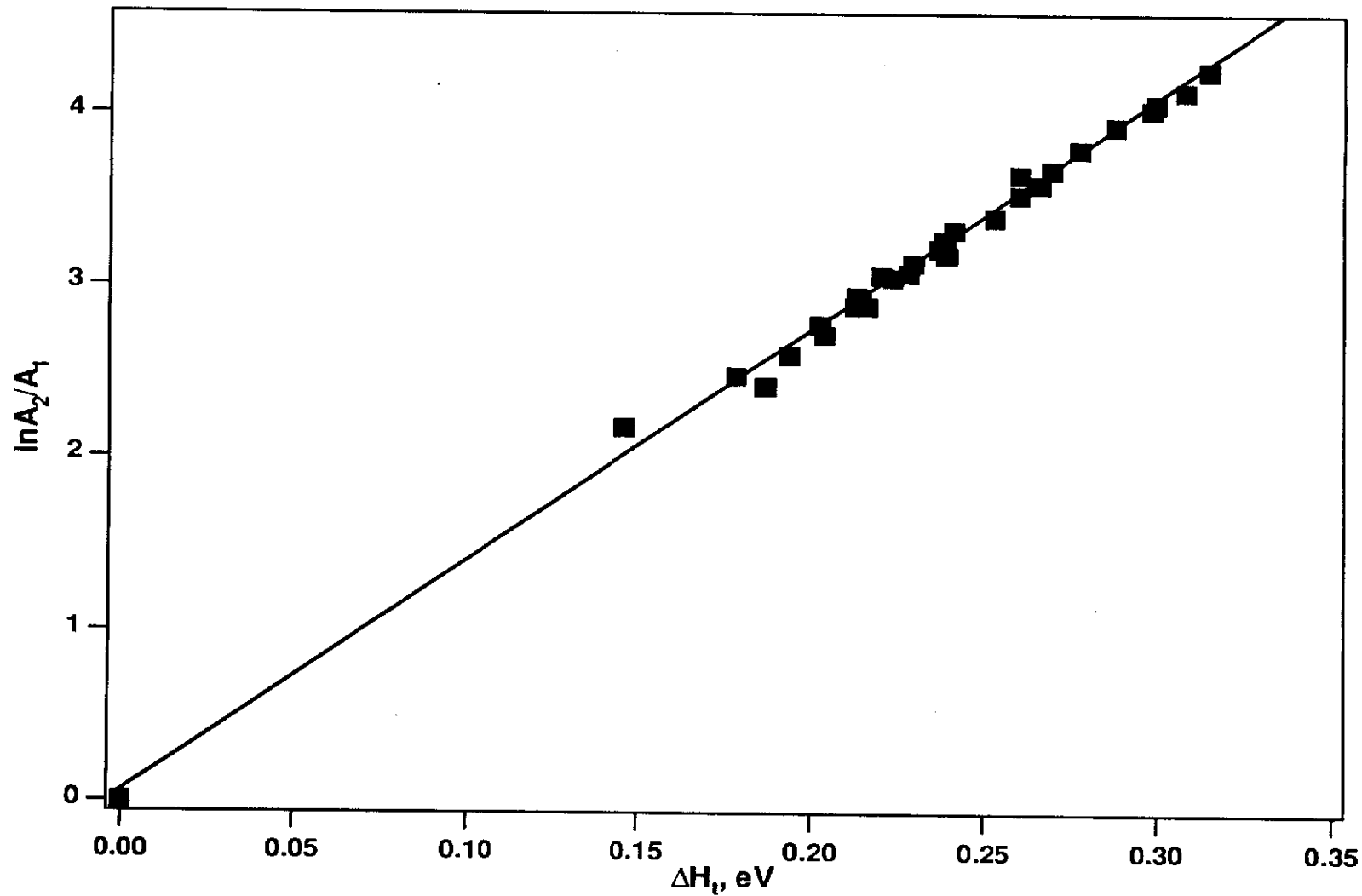
$$\mu_V^*(\text{cond}) = \mu_V^*(\text{sol}) = \mu_V^0(\text{sol}) + kT \ln(c/c^*)$$

Since  $\Delta G_t(T^*) = 0$

$$\begin{aligned} \ln(c/c^*) &= -[\Delta G_t(T)/kT - \Delta G_t(T^*)/kT^*] \\ &= -\Delta H_t(1-T/T^*)/kT \end{aligned}$$

Note:  $T^* = 599 \pm 49$  °C for all samples

$\ln A_2 / A_1$  vs  $\Delta H_t$



# INFLUENCE OF DOPING METHOD

---

If method of doping, *i. e.*, Sr for La vs Mg for Ga, to obtain a given  $c^*$  effects  $\Delta H_t$ , but not  $\Delta H_m$  or  $T^*$ , then:

$\ln(\sigma_0 T)$  vs  $(1/T)$  is  $\left\{ \begin{array}{l} \text{common for } T \geq T^* \\ \text{diverges for } T < T^* \end{array} \right.$

# MEYER-NELDER RULE

## OBEYED $T < T^*$

---

For some semiconductors with  $\sigma_0 T = A \exp(-E_a/kT)$

$$\ln A = aE_a + b$$

is found empirically. In our case with  $T \leq T^*$ ,

$$\sigma_0 T = B \exp(-E_2/kT)$$

$$\sigma_0 T^* = B \exp(-E_2/kT^*) = A \exp(-\Delta H_m/kT^*)$$

$$\therefore \ln B = aE_2 + b$$

with  $E_2 = \Delta H_m + \Delta H_t$ ,  $a = 1/kT^*$ ,  $b = \ln A - (\Delta H_m/kT^*)$

# MOBILITY & DIFFUSIVITY

For  $T \geq T^*$

$$\sigma_O = c^* N q \mu_O = 2 e c^* \mu_O / a^3 = (A/T) \exp(-\Delta H_m / kT)$$

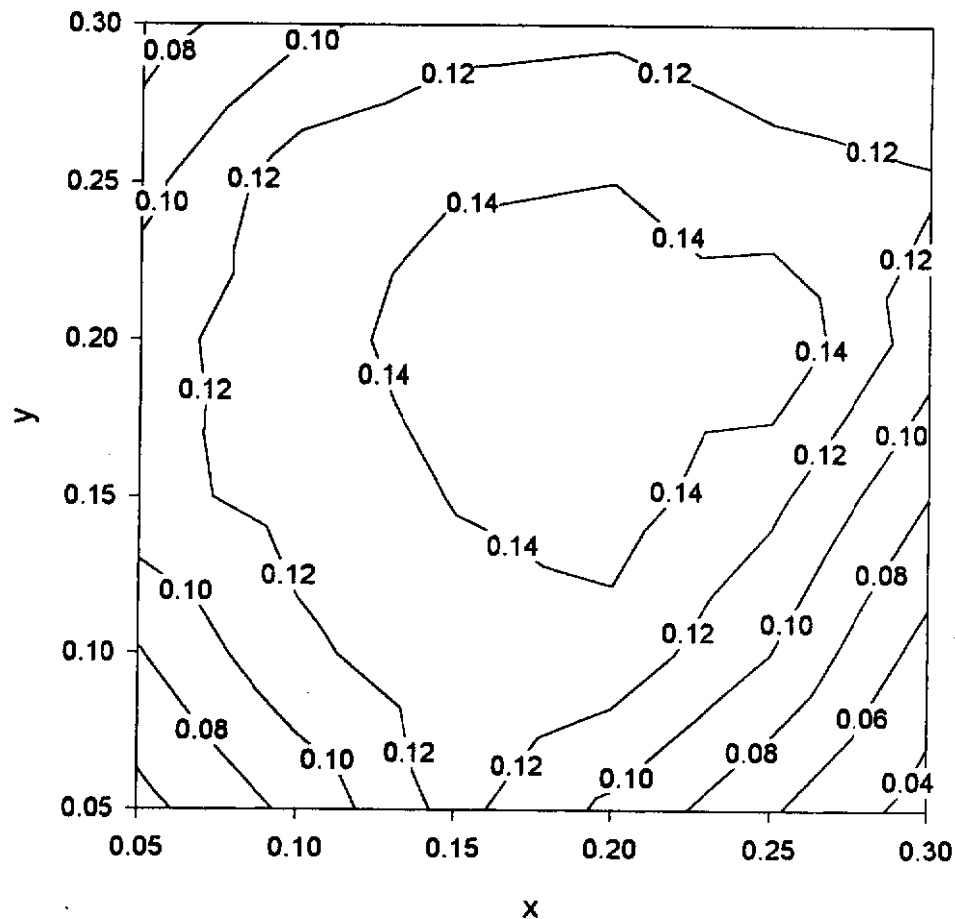
$$\therefore \mu_O \exp(\Delta H_m / kT) = A a^3 / 2 e c^* T = e D_O / kT$$

We measure  $\Delta H_m$ ,  $A$ , lattice constant  $a$ ,  $c^*$  to obtain:

Sample		$c^*$	$\mu_O, \times 10^{-5} \text{cm}^2/\text{Vs}$			$D_O, \times 10^{-6} \text{cm}^2/\text{s}$		
x	y		600	700	800 °C	600	700	800 °C
0.15	0.15	0.05	8.72	26.3	53.9	3.29	11.0	24.9
0.15	0.20	0.06	7.16	22.9	49.2	2.70	9.60	22.8
0.20	0.15	0.06	8.12	23.8	48.7	3.06	9.98	22.6

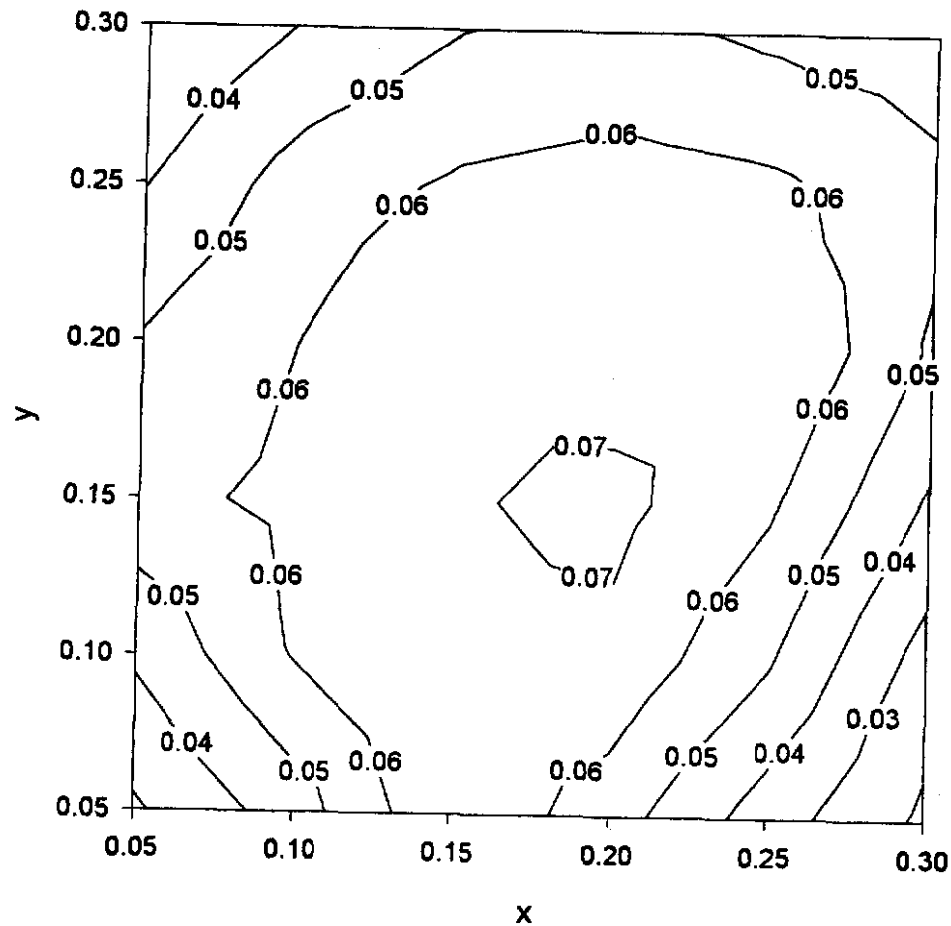
# Isoconductivity Contours at 800 °C (S/cm)

for  $\text{La}_{1-x}\text{Sr}_x\text{Ga}_{1-y}\text{Mg}_y\text{O}_{3-0.5(x+y)}$



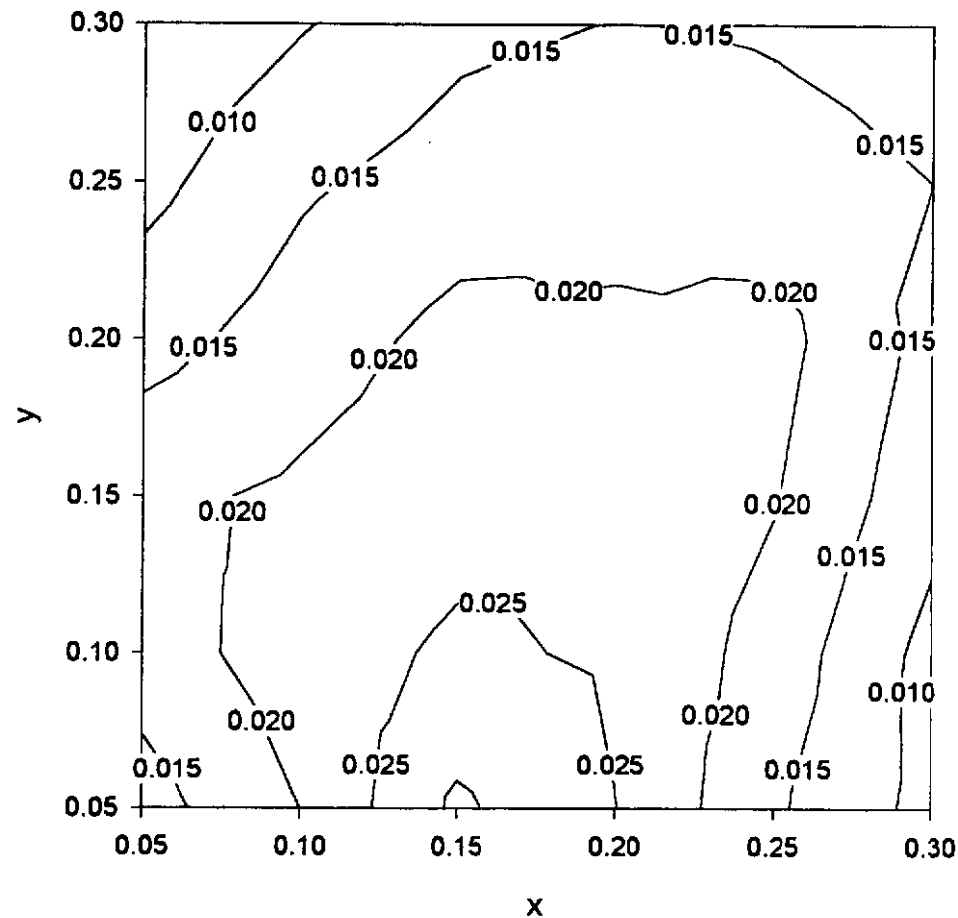
# Isoconductivity Contours at 700 °C (S/cm)

for  $\text{La}_{1-x}\text{Sr}_x\text{Ga}_{1-y}\text{Mg}_y\text{O}_{3-0.5(x+y)}$

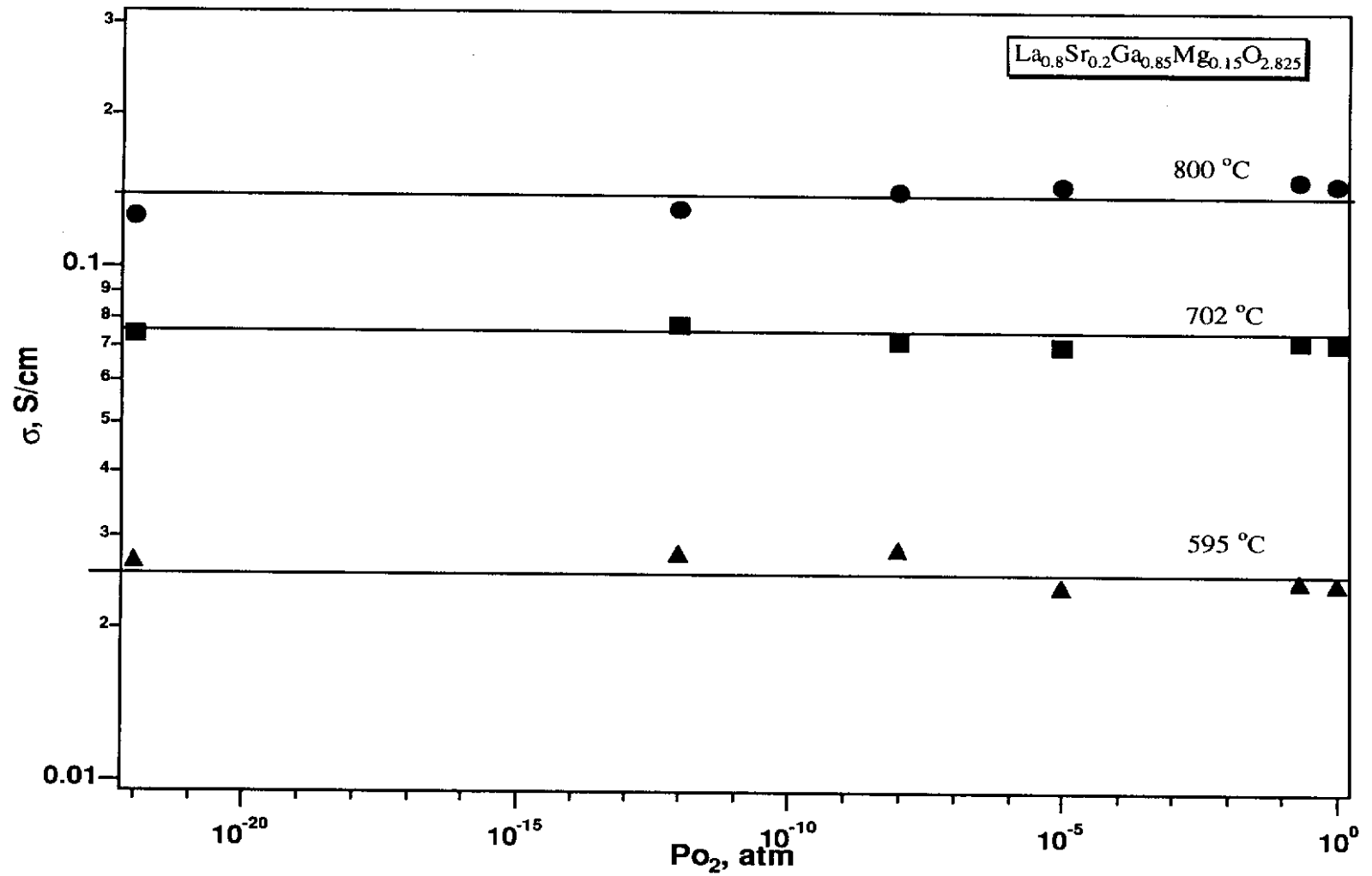


# Isoconductivity Contours at 600 °C (S/cm)

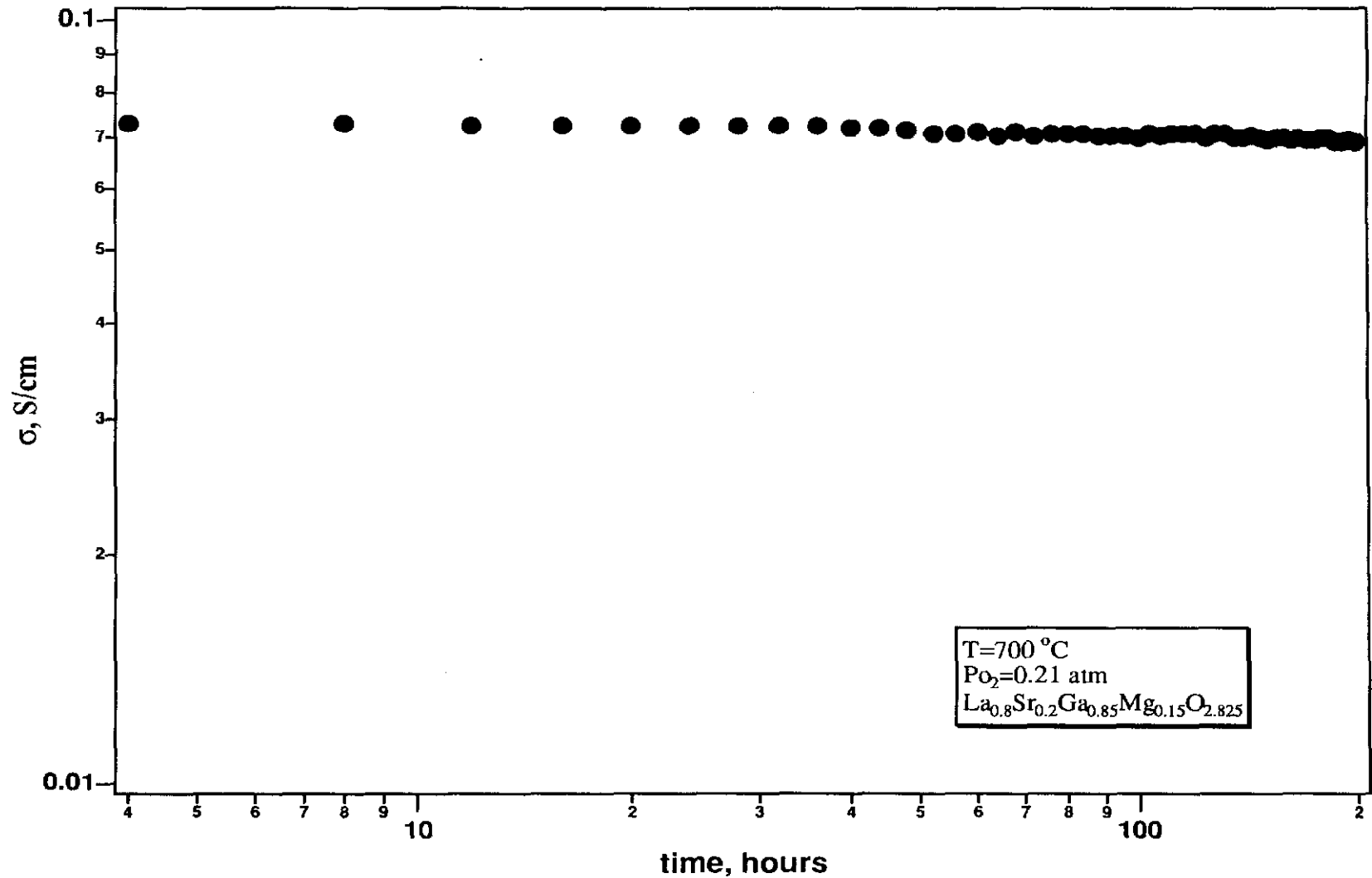
for  $\text{La}_{1-x}\text{Sr}_x\text{Ga}_{1-y}\text{Mg}_y\text{O}_{3-0.5(x+y)}$



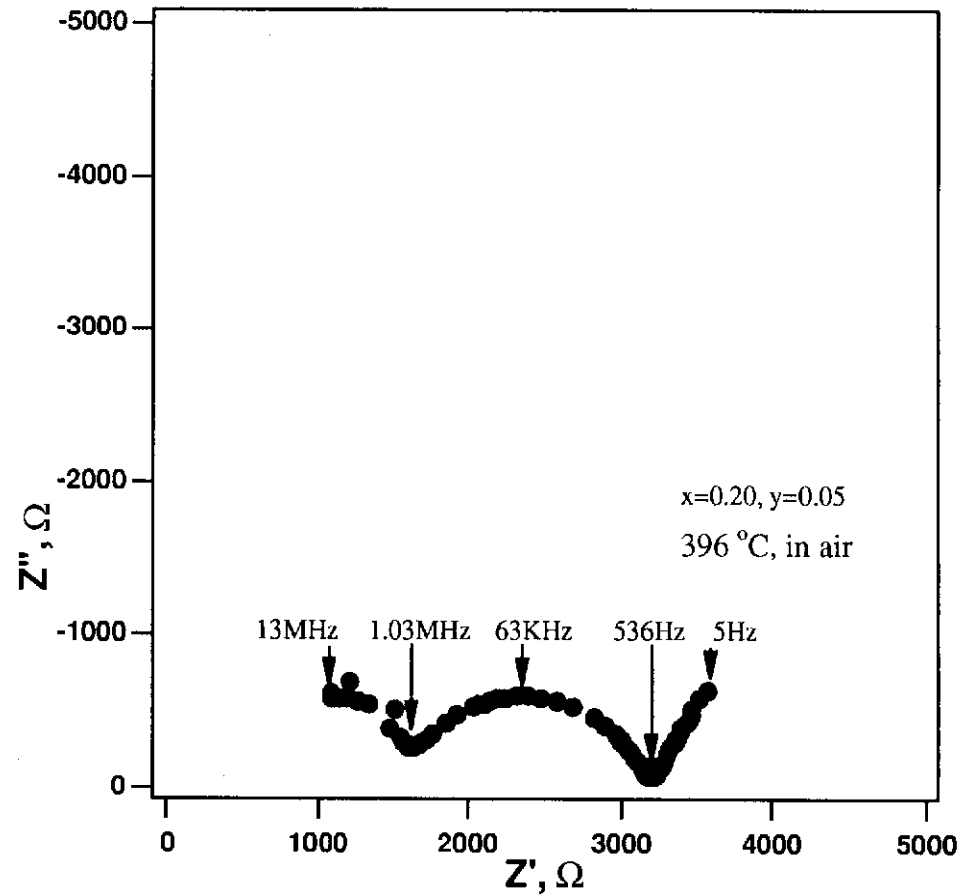
# Conductivity vs $P_{O_2}$



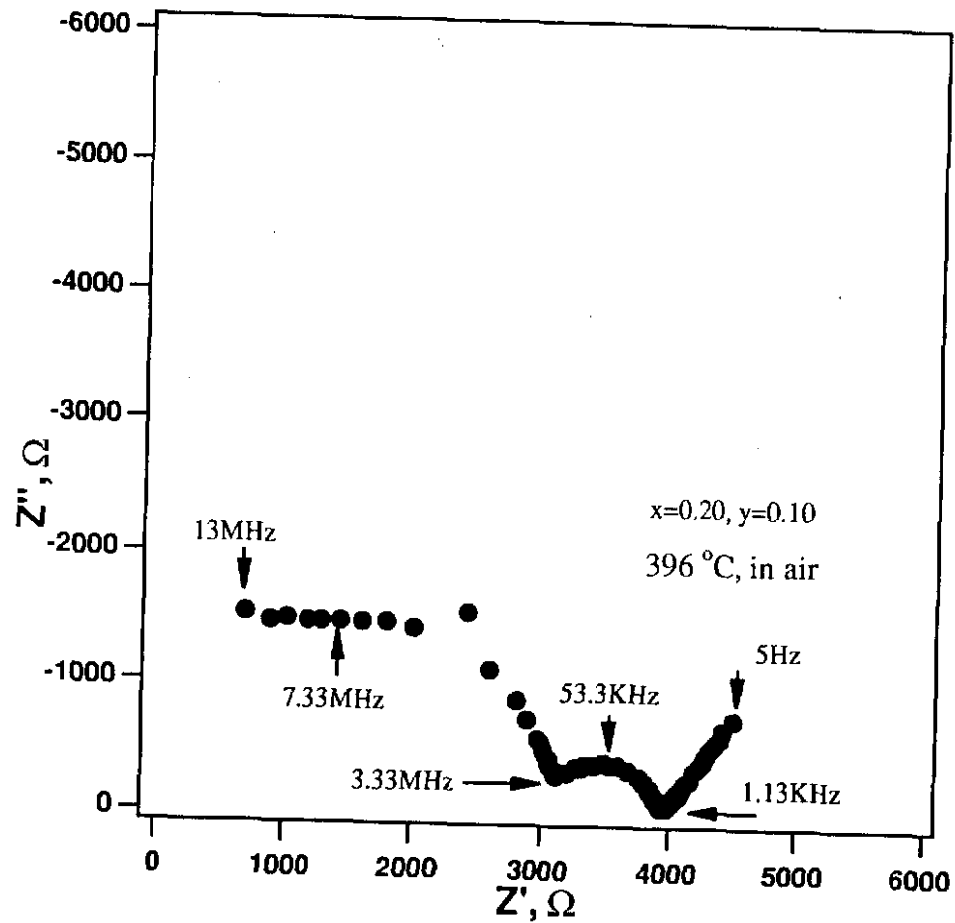
# Conductivity vs time



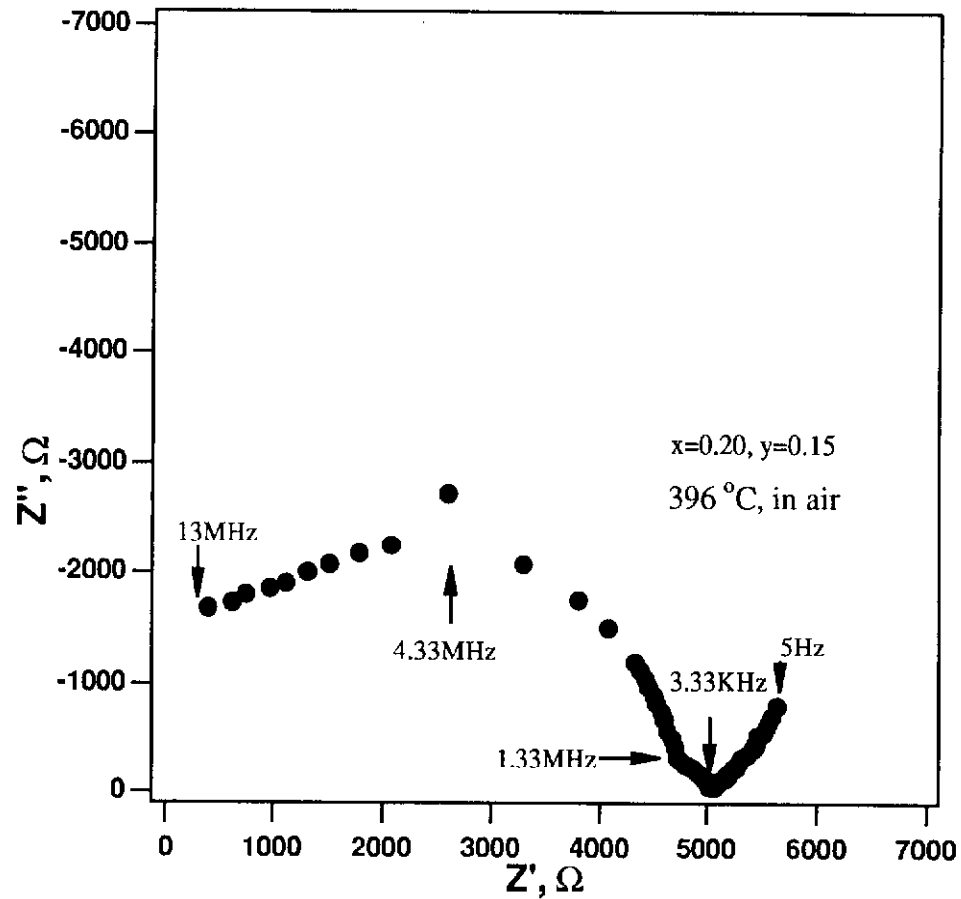
# Impedance Spectrum



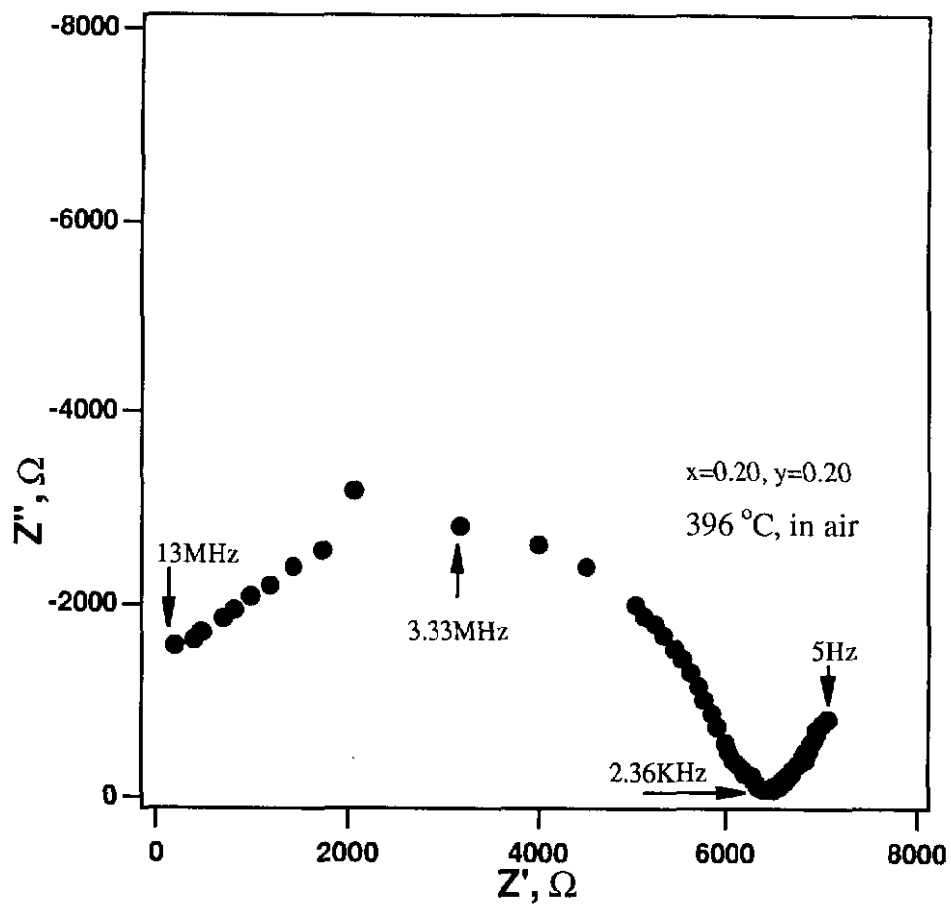
# Impedance Spectrum



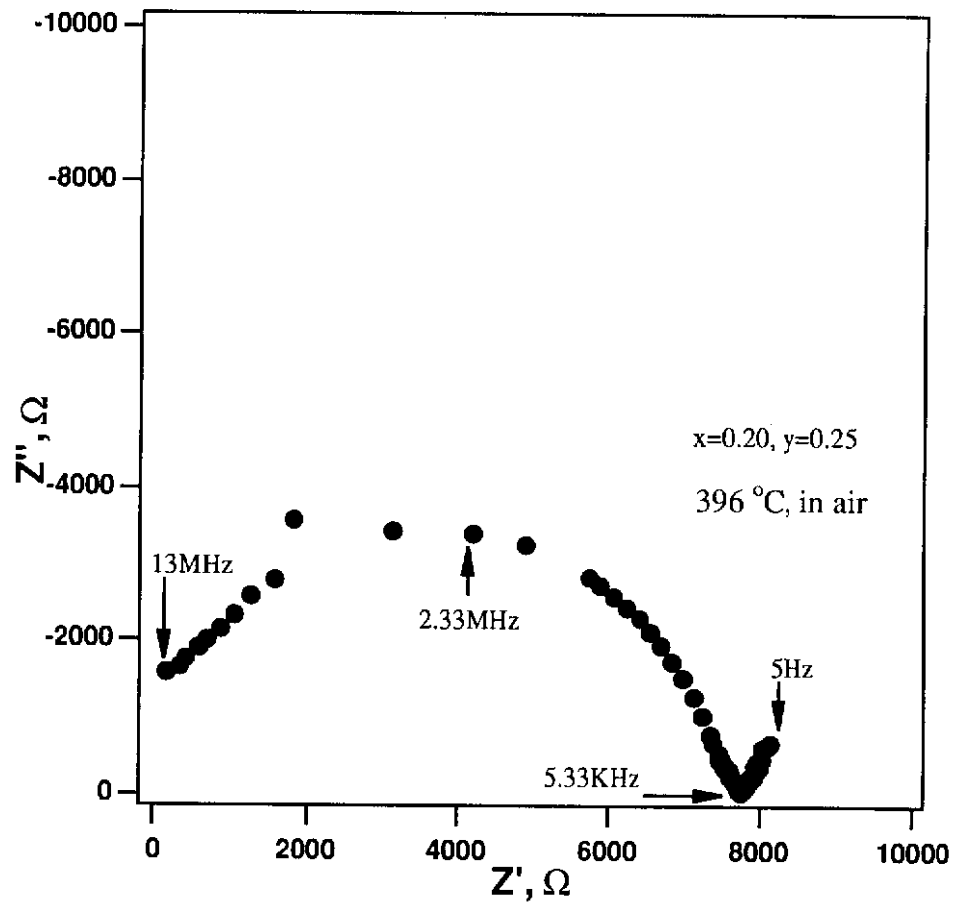
# Impedance Spectrum



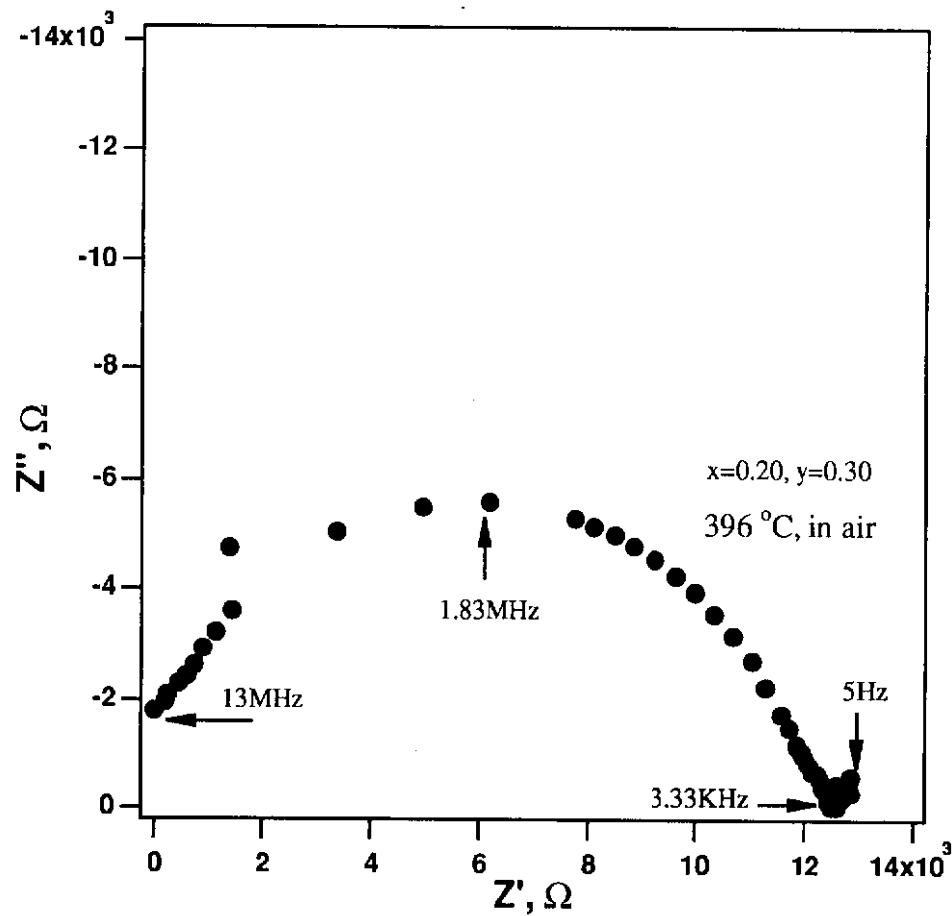
# Impedance Spectrum



# Impedance Spectrum

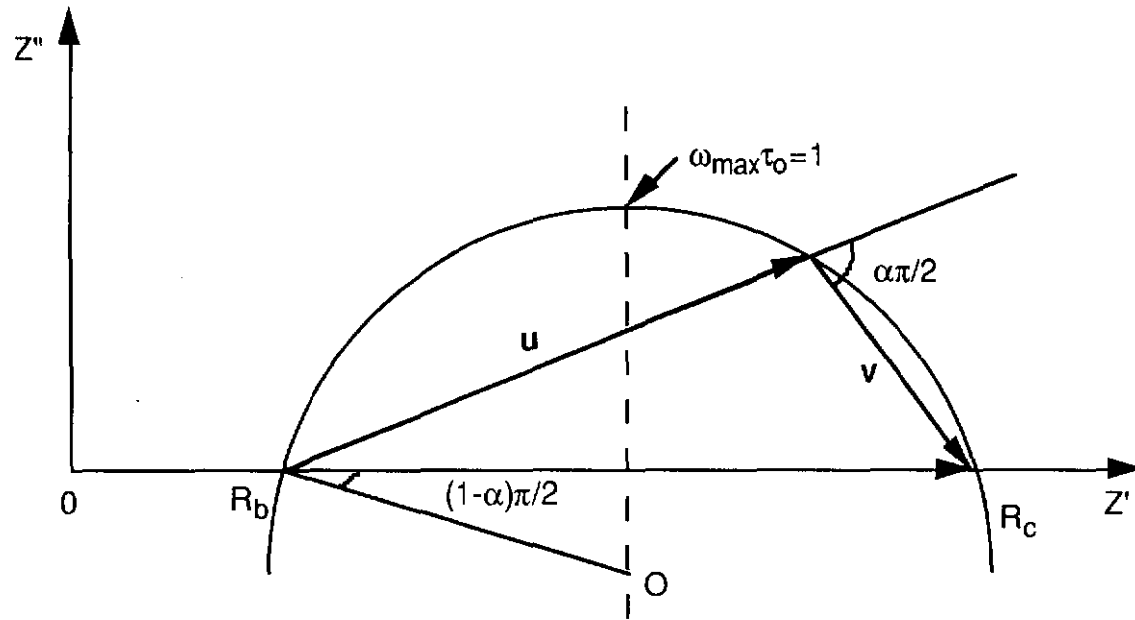


# Impedance Spectrum



# A Graphic Presentaion of CPE

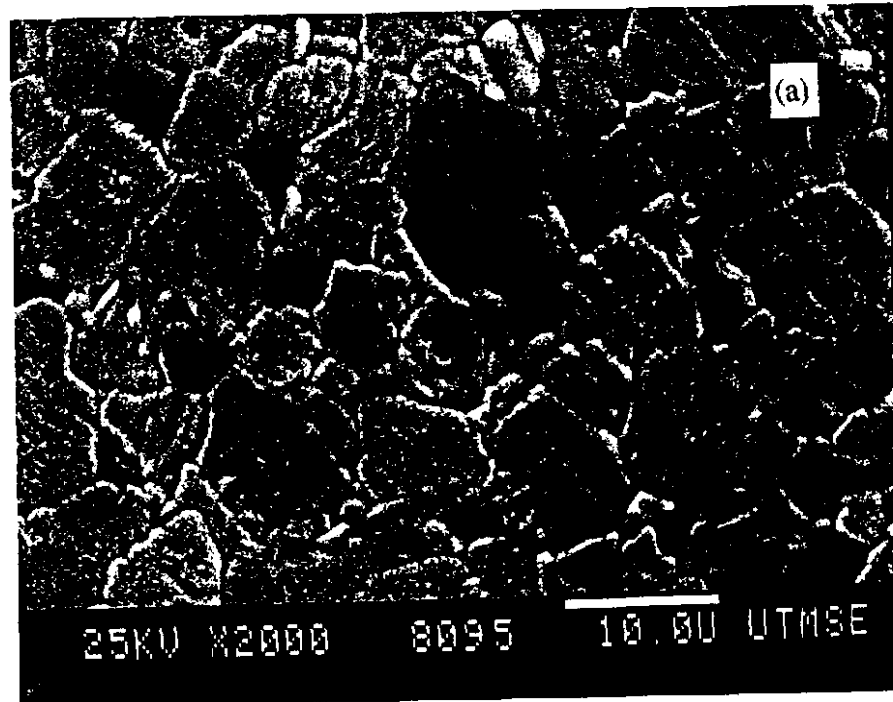
---



# SEM Microstructures

$x=0.2, y=0.05$

---

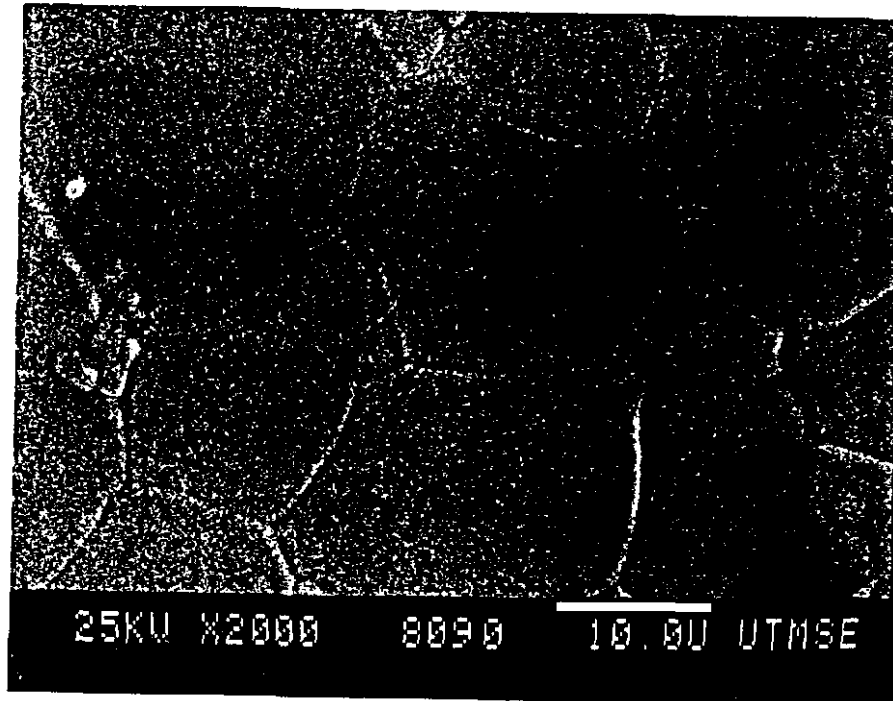


thermal etch at 1350 °C for 1 h

# SEM Microstructures

$x=0.2, y=0.1$

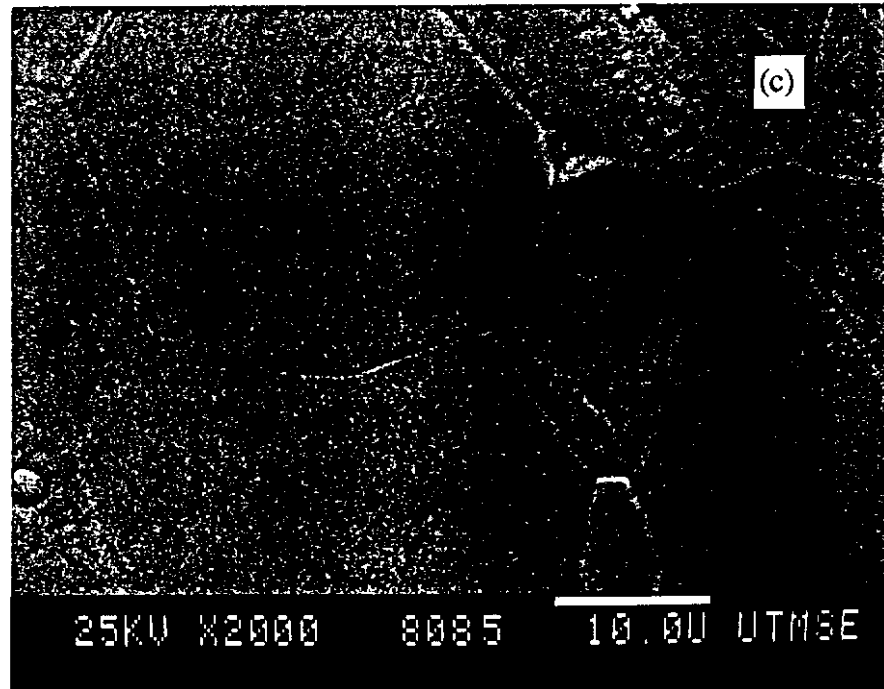
---



# SEM Microstructures

$x=0.2, y=0.15$

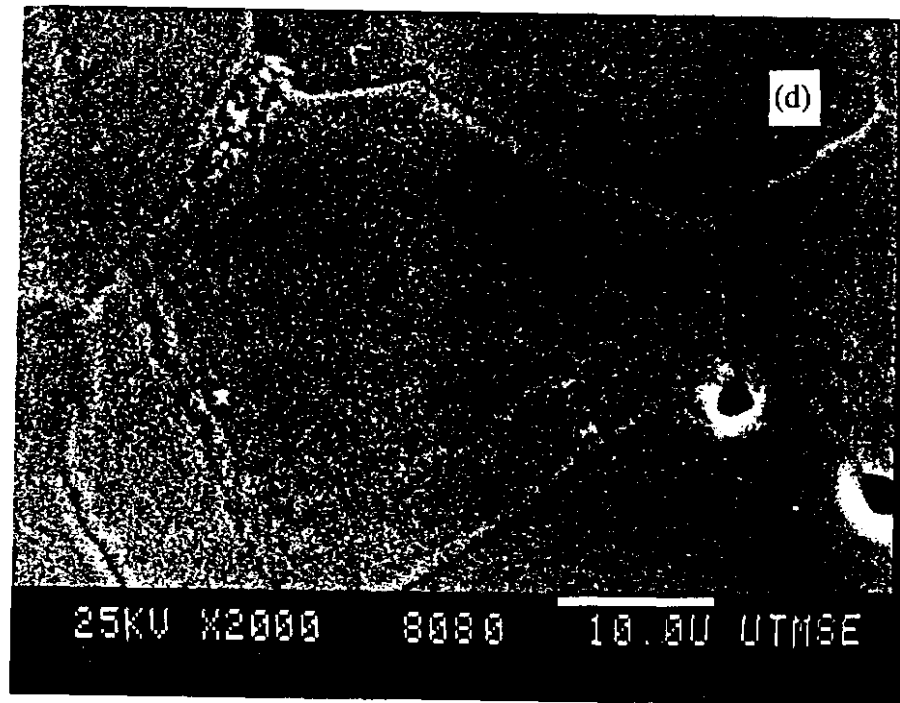
---



# SEM Microstructures

$x=0.2, y=0.2$

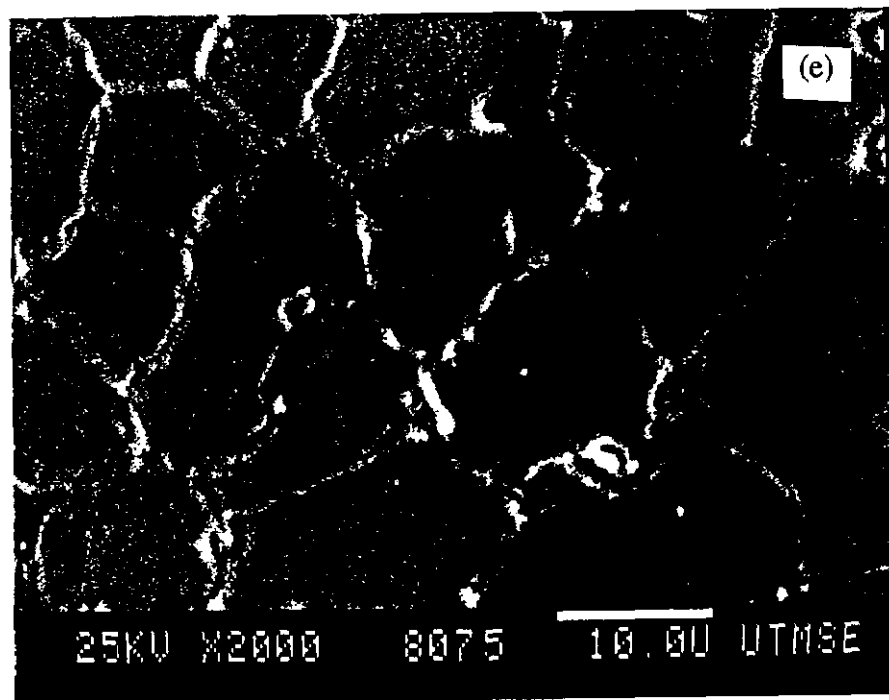
---



# SEM Microstructures

$x=0.2, y=0.25$

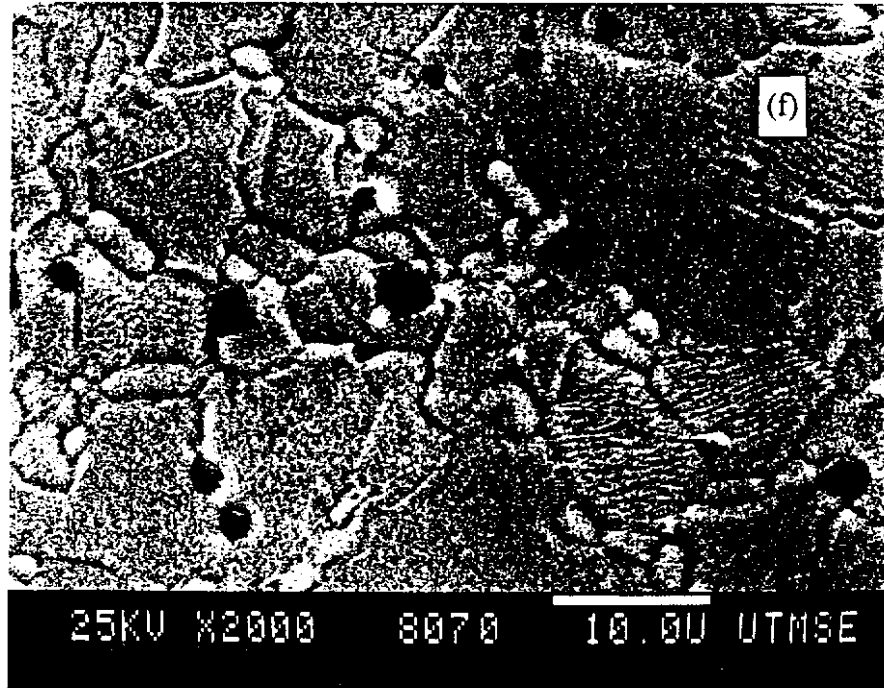
---



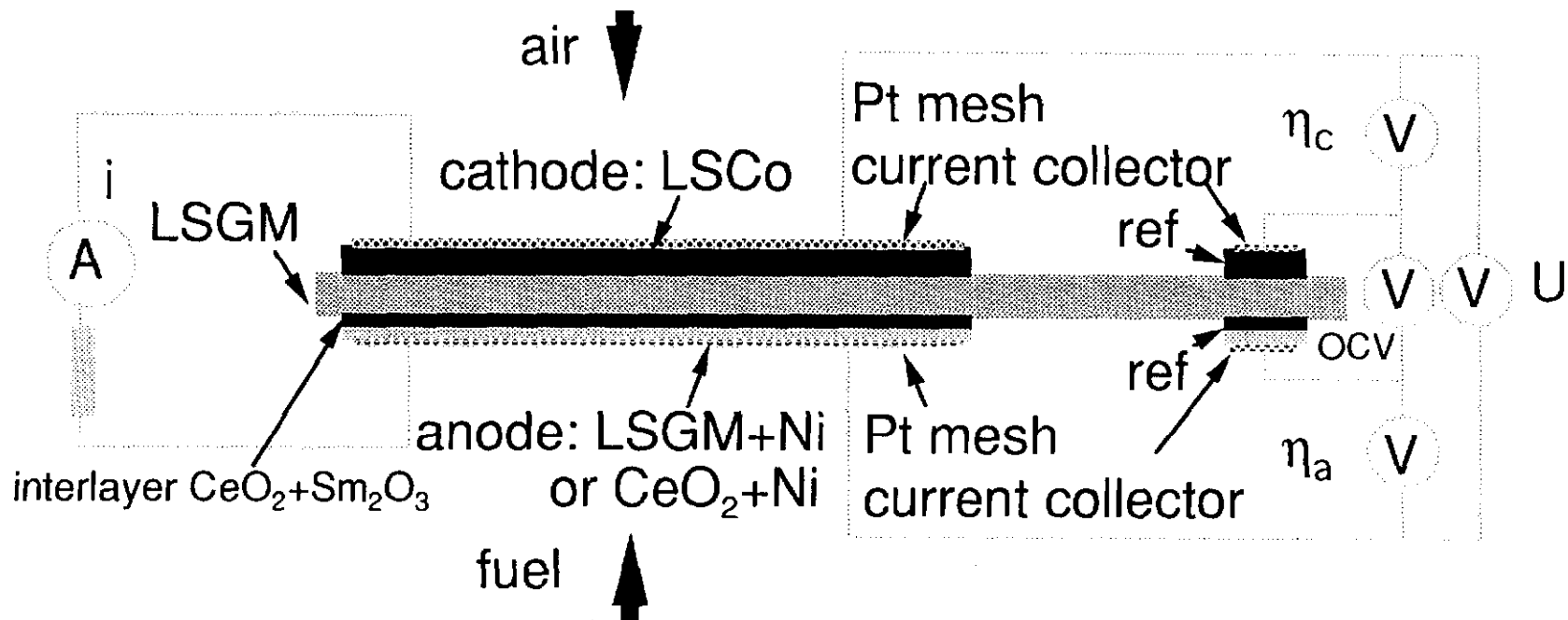
# SEM Microstructures

$x=0.2, y=0.3$

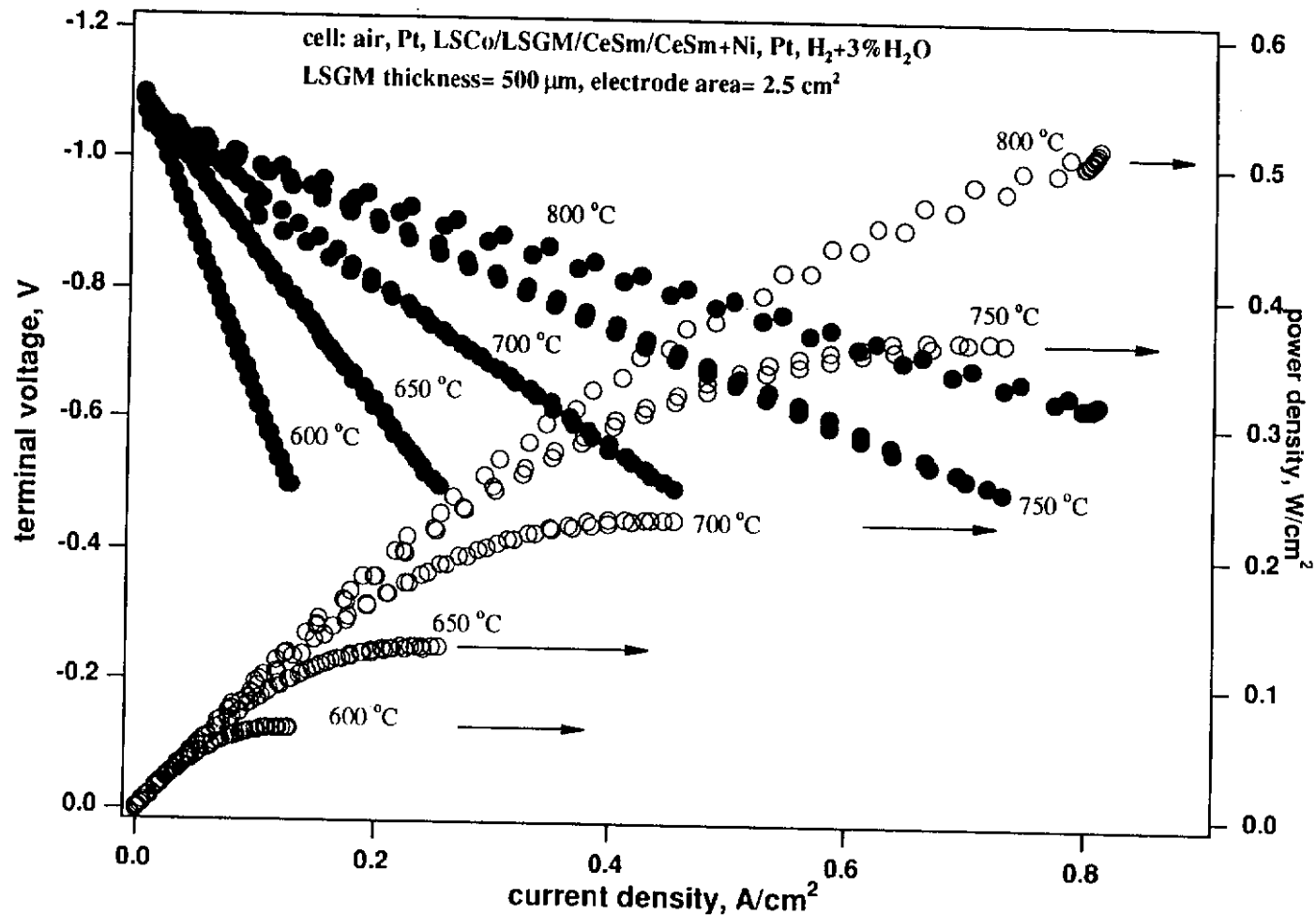
---



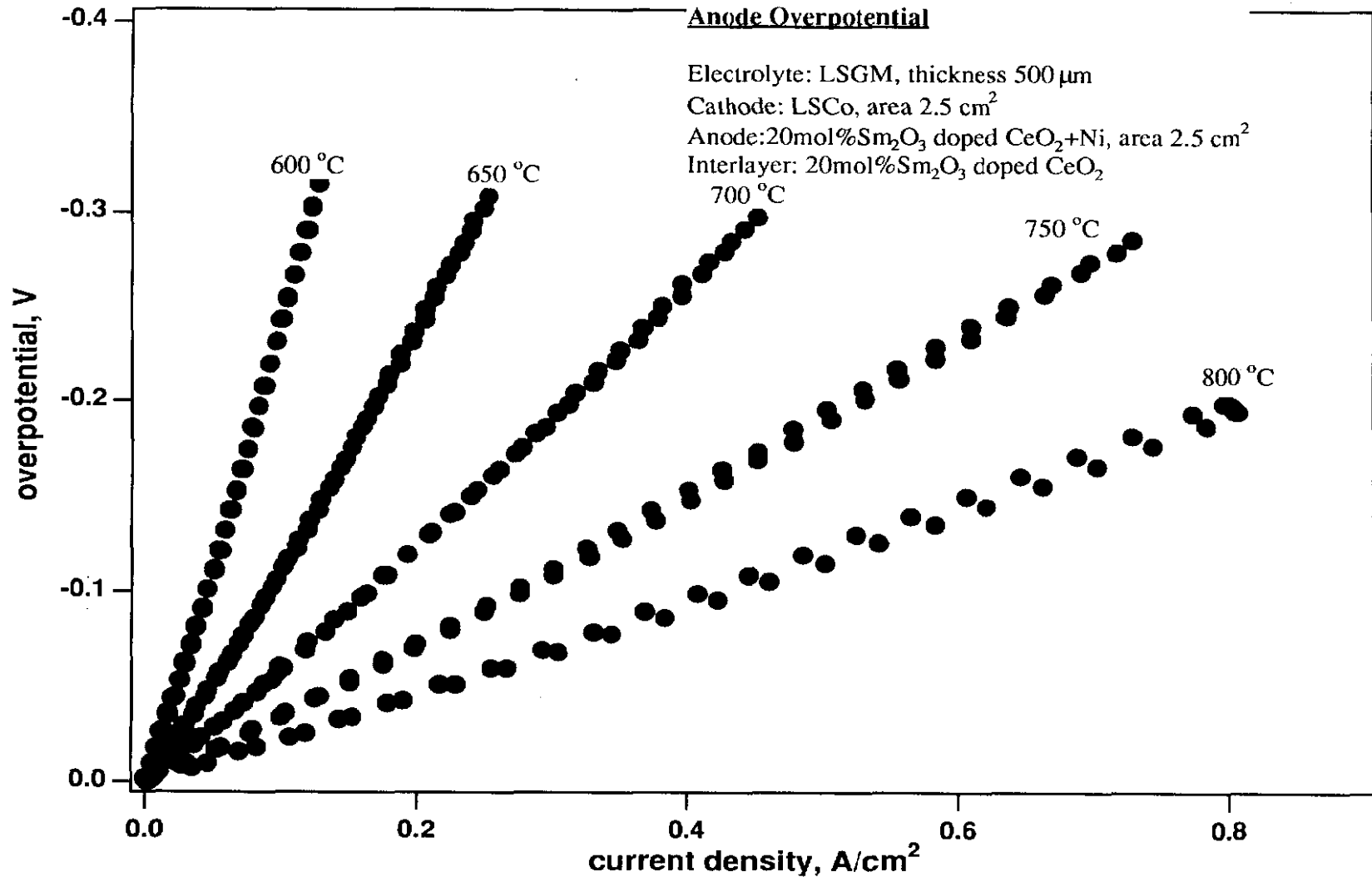
# Single Fuel Cell Configuration



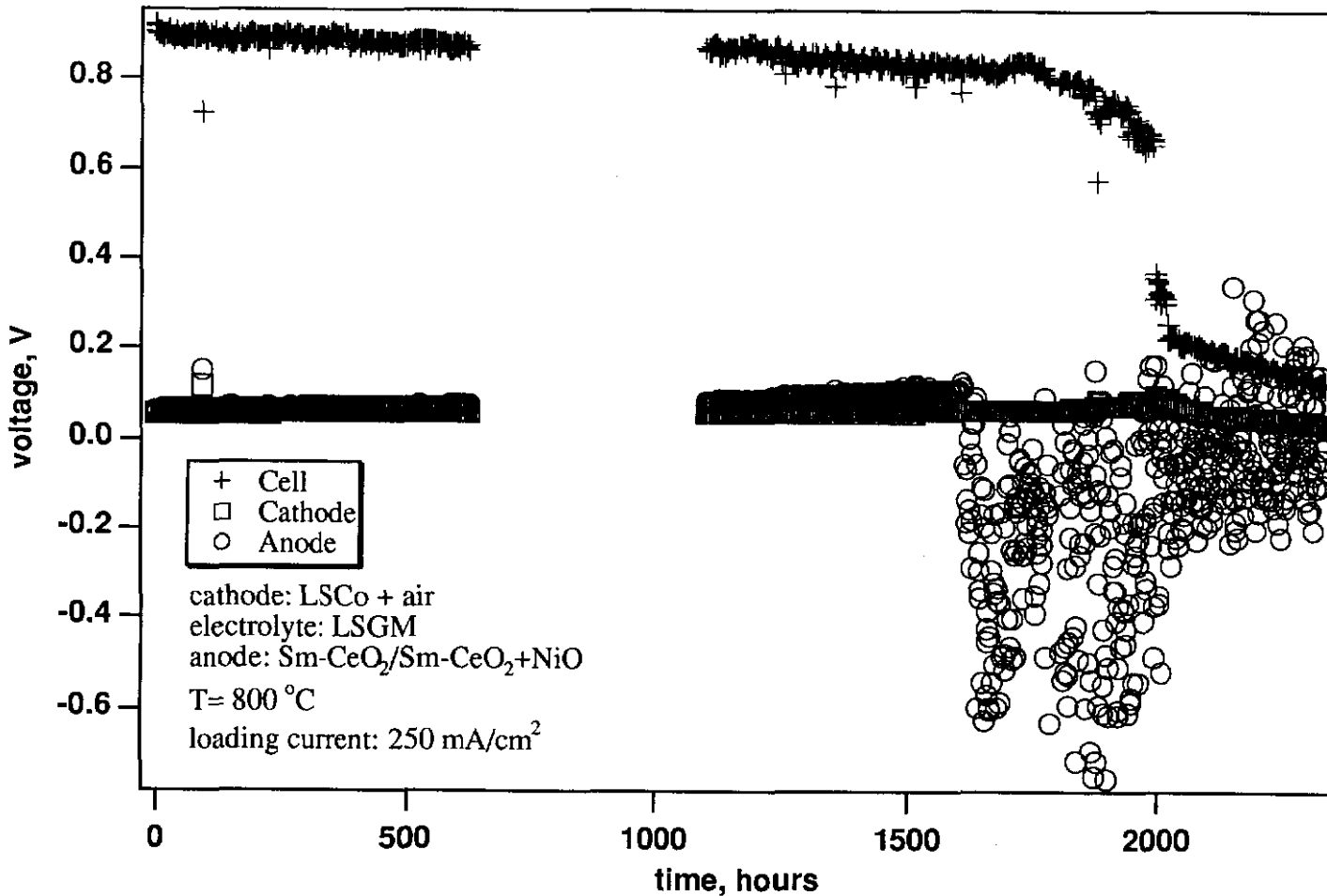
# Performance of Fuel Cell with Buffer-layer



# Anode Overpotential vs Current Density



# Preliminary Life Test for 500 $\mu\text{m}$ LSGM Electrolyte



# CONCLUSION

---

With the addition of a doped ceria anode buffer layer, the realization of a SOFC based on an LSGM electrolyte operating in the range  $600^{\circ}\text{C} < T_{\text{op}} < 800^{\circ}\text{C}$  is a realistic goal.